Hot Spring Microbial Community Composition, Morphology, and Carbon Fixation: Implications for Interpreting the Ancient Rock Record

Caleb G. Schuler[1†], Jeff R. Havig[2†] and Trinity L. Hamilton[1*†]

[1] Department of Biological Sciences, University of Cincinnati, Cincinnati, OH, United States, [2] Department of Geology, University of Cincinnati, Cincinnati, OH, United States

Microbial communities in hydrothermal systems exist in a range of macroscopic morphologies including stromatolites, mats, and filaments. The architects of these structures are typically autotrophic, serving as primary producers. Structures attributed to microbial life have been documented in the rock record dating back to the Archean including recent reports of microbially-related structures in terrestrial hot springs that date back as far as 3.5 Ga. Microbial structures exhibit a range of complexity from filaments to more complex mats and stromatolites and the complexity impacts preservation potential. As a result, interpretation of these structures in the rock record relies on isotopic signatures in combination with overall morphology and paleoenvironmental setting. However, the relationships between morphology, microbial community composition, and primary productivity remain poorly constrained. To begin to address this gap, we examined community composition and carbon fixation in filaments, mats, and stromatolites from the Greater Obsidian Pool Area (GOPA) of the Mud Volcano Area, Yellowstone National Park, WY. We targeted morphologies dominated by bacterial phototrophs located in close proximity within the same pool which are exposed to similar geochemistry as well as bacterial mat, algal filament and chemotrophic filaments from nearby springs. Our results indicate (i) natural abundance $\delta^{13}C$ values of biomass from these features (−11.0 to −24.3‰) are similar to those found in the rock record; (ii) carbon uptake rates of photoautotrophic communities is greater than chemoautotrophic; (iii) oxygenic photosynthesis, anoxygenic photosynthesis, and chemoautotrophy often contribute to carbon fixation within the same morphology; and (iv) increasing phototrophic biofilm complexity corresponds to a significant decrease in rates of carbon fixation—filaments had the highest uptake rates whereas carbon fixation by stromatolites was significantly lower. Our data highlight important differences in primary productivity between structures despite indistinguishable $\delta^{13}C$ values of the biomass. Furthermore, low primary productivity by stromatolites compared to other structures underscores the need to consider a larger role for microbial mats and filaments in carbon fixation and O_2 generation during the Archean and Proterozoic.

Keywords: stromatolites, hot springs, carbon uptake, oxygenic photosynthesis, cyanobacteria

INTRODUCTION

Physical structures of extant microbial communities include filaments, microbial mats, and stromatolites. These structures are common in a range of environments including hydrothermal features and are comprised of diverse microbial assemblages. Filaments, microbial mats, and stromatolites have been found in the ancient rock record (e.g., Logan et al., 1964; Schopf, 1993; Allwood et al., 2006; Noffke et al., 2006; Schopf et al., 2007) and provide evidence for the presence of life including the recent discovery of microbial structures in terrestrial hydrothermal systems dating to 3.5 Ga (Djokic et al., 2017). Unfortunately, microbial life left a poor fossil record and examples of taxa-specific biosignatures and morphologies are rare, hindering our interpretation of these structures in the rock record. For instance, taxonomic or morphological signatures could aid in determining the prevailing environmental conditions and biogeochemical cycling at the time of formation and deposition.

Methods of interpreting microbial signatures in the rock record rely on recovery of biosignatures (e.g., lipids, pigments), isotopic signatures, and morphology. Recently, biosignature records of Archean rocks have been called in to question due to contamination (French et al., 2015) whereas similar morphologies exist in drastically different environments. Based on similarities with mats, stromatolites and filaments formed by extant cyanobacteria, these structures are often inferred to be of cyanobacterial origin. However, extant structures are often comprised of taxonomically and metabolically diverse organisms. In addition, mat and filament formation can proceed in the absence of cyanobacteria. For instance, filaments and microbial mats have been observed in cave systems in the absence of light (e.g., Engel et al., 2003, 2004; Macalady et al., 2006; Northup et al., 2011), near deep-sea hydrothermal vents (e.g., Jannasch and Wirsen, 1981; Kato et al., 2009), and in geothermal springs where geochemical conditions or temperature preclude photosynthesis (e.g., Havig et al., 2011). Similar to morphological identification, carbon isotope fractionation can be ambiguous—carbon fixation pathways of photoautotrophs and chemoautotrophs can produce biomass that is indistinguishable (e.g., Havig et al., 2011, 2017).

Recent work has highlighted the microscopic and macroscopic morphological similarities between stromatolites growing in silica-saturated hot springs and ancient stromatolites (e.g., Berelson et al., 2011; Mata et al., 2012; Pepe-Ranney et al., 2012; Spear and Corsetti, 2013). And, microbial structures including stromatolites and microbial palisade fabric have been inferred in silica-rich terrestrial hydrothermal systems dating to 3.5 Ga (Djokic et al., 2017). These observations underscore the need to better understand the microbial communities forming these structures in modern geothermal settings. Microbial mats and filaments are less likely to be observed in ancient rocks because fossilization requires lithification/mineralization of these relatively delicate structures. Still, the prevalence of mats and filaments in modern environments is much more widespread compared to actively growing stromatolites, which are rare.

Ancient oceans are thought to have been near saturation with respect to silica (Maliva et al., 2005), and the best preservation of filaments, mats, and stromatolites is correlated with early silicification (e.g., Oehler and Schopf, 1971; Hofmann, 1975; Knoll, 1985; Southgate, 1986; Konhauser et al., 2003). Yellowstone National Park (YNP) contains an estimated 10,000 thermal features, most of which are hosted in rhyolitic tuffs and lava flows resulting from sub-continental plate hot spot volcanism. Rhyolite is a felsic igneous rock and contains a high percentage of silica (>69%). As a result, geothermal springs in and near the 640,000 year old caldera in YNP are typically silica-saturated (Fournier, 1989) and serve as a proxy for ancient oceans at or near silica saturation. In addition, silica-saturated geothermal systems like those in YNP are ideal locations for understanding early life because: (1) there is evidence for the presence of geothermal systems throughout Earth's history (e.g., Djokic et al., 2017; Dodd et al., 2017); (2) they often harbor deep-branching microbes (Pace, 1997; Reysenbach and Shock, 2002); and (3) physicochemical conditions of the hydrothermal water excludes multicellular life enabling the formation (and preservation) of microbial structures in the absence of grazing. The Greater Obsidian Pool Area (GOPA) in the Mud Volcano Area of YNP contains silica-rich geothermal springs that are host to filamentous and microbial mat communities as well as stromatolites. A number of deep-branching 16S rRNA sequences have been recovered from GOPA (Barns et al., 1994, 1996; Hugenholtz et al., 1998; Meyer-Dombard et al., 2005) and the siliceous stromatolites of Obsidian Pool Prime (OPP) have been previously characterized (Berelson et al., 2011; Mata et al., 2012; Pepe-Ranney et al., 2012). Thus, GOPA is an excellent setting for characterizing the microbial community composition and productivity of extant microbial structures to inform interpretation of these structures in the ancient rock record.

Here, we determined community composition and primary productivity in filaments, mats, and stromatolites in GOPA. We chose mats, filaments, and stromatolites located in close proximity in the same pool to constrain physical and geochemical parameters. In addition, we examined the same characteristics in biofilms from three nearby springs with distinct geochemistry. Rates of carbon fixation were highest in filaments and mats dominated by cyanobacterial 16S rRNA sequences; however, oxygenic and anoxygenic photosynthesis as well as chemoautotrophy can contribute to carbon fixation within the same morphology. Increasing phototrophic biofilm complexity corresponded with a significant decrease in rates of carbon fixation—filaments exhibited the highest uptake rates and stromatolites the lowest uptake rates. Our natural abundance $\delta^{13}C$ values of biomass from these features (−11.0 to −24.3‰) are similar to those found in the rock record. Our data indicate stromatolites are less productive than filaments and mats, suggesting mats and filaments have played a larger role in biogeochemical cycling, particularly carbon fixation and oxygen production, throughout Earth's history despite their paucity in the rock record.

MATERIALS AND METHODS
Field Site Description

The Greater Obsidian Pool Area (GOPA) of the Mud Volcano Area, Yellowstone National Park, WY is a hydrothermal area

rich with biodiversity and geothermal features. The geothermal features vary in temperature, pH, as well as geochemical properties such as the concentration of sulfide and chloride. GOPA itself is roughly 1 km^2 and drains into Goose Lake and its outflow stream to the north. Due to the rich biodiversity and geochemical gradients, GOPA is often used as a study site for microbial phylogenetics as well as geothermal research (Barns et al., 1994; Hugenholtz et al., 1998; Meyer-Dombard et al., 2005; Shock et al., 2005; Spear et al., 2005; Havig, 2009; Berelson et al., 2011; Mata et al., 2012; Pepe-Ranney et al., 2012).

Microbial Community Morphology Descriptions

The microbial communities sampled in Yellowstone National Park fell into three primary morphologies: filaments, mats, and stromatolites. Here we use the term filaments to include microbial community structures that are predominantly filamentous at the macro-scale, and are strictly subaqueous. Mats are layered microbial communities that form a continuous coherent mass of uniform thickness, and can be either subaqueous or found at the water-air interface. Stromatolites are layered microbial structures that form at the water-air interface, but then grow subaerially. There were three filament communities sampled (Sites 1A, 3, and 4), three mat communities sampled (Sites 1B, 1C, and 2), and one stromatolite community (Site 1D) (**Figure 1**).

Sample Collection and Geochemistry

All measurements, samples, and *in situ* microcosms (described below) were performed and collected on July 22, 2016 except the natural abundance sample for the stromatolite (described in more detail below). Samples for nucleic acid extraction ($n = 3$) and C and N content and $\delta^{13}C$ determination ($n = 1$) were collected using flame-sterilized spatulas or forceps. Samples were placed in sterile 1.5 mL vials and immediately frozen on dry ice and stored at $-80°C$ until nucleic acid extraction or C, N and $\delta^{13}C$ analysis. Temperature and pH were measured onsite using a WTW 330i meter and probe (Xylem Analytics, Weilheim, Germany) and conductivity was measured with a YSI 30 conductivity meter and probe (YSI Inc., Yellow Springs, OH, USA). Sulfide, Fe^{2+} and dissolved silica were measured onsite using a DR1900 portable spectrophotometer (Hach Company, Loveland, CO).

Water samples were filtered through 25 mm diameter 0.2 μm polyethersulfone syringe filters (VWR International, Radnor, PA, USA). For ion chromatography analysis of anions, water was filtered into 15-mL centrifuge tubes (pre-soaked in 18.2 MΩ/cm DI water). Samples were stored at $4°C$ until analysis. Major anions (fluoride, chloride, sulfate, and nitrate) were determined using a Dionex ICS2500 ion chromatography (IC) system (Dionex, Sunnyvale, CA, USA) by the Earth and Environmental Systems Institute (EESI) (The Pennsylvania State University, University Park, PA, USA) as described previously (Havig et al., 2015). Samples for cation (sodium, potassium, calcium, and magnesium) analysis were filtered into acid-washed 15-mL centrifuge tubes (3 day soak in 10% TraceMetal Grade HNO_3 (Fisher Scientific, Hampton, NH, USA) followed by triple rinsing

with 18.2 MΩ/cm DI water) and immediately acidified with 400 μL of concentrated OmniTrace Ultra™ concentrated nitric acid (EMD Millipore, Billerica, MA, USA). Samples were stored at $4°C$ until analysis. Analysis of cations was conducted via Thermo X-Series II Quadrupole collision cell technology enabled inductively-coupled plasma mass spectrometer (Thermo Fisher Scientific, Waltham, MA, USA) by the EESI at the Pennsylvania State University as described previously (Havig et al., 2015). Field blanks comprised of filtered 18.2 MΩ/cm deionized water transported to the field in 1-liter Nalgene bottles (acid-washed as described above) were collected onsite using the same equipment and techniques described above.

4-mL samples for dissolved inorganic carbon (DIC) concentration analysis were filtered into Labco Exetainers® (Labco Limited, Lampeter, UK) pre-flushed with helium. Samples were stored cap-side down at $4°C$ until analysis. DIC concentrations and $\delta^{13}C$ were determined by the Stable Isotope Facility at University of California, Davis using a GasBench II system interfaced to a Delta V Plus isotope ratio mass spectrometer (IR-MS) (Thermo Scientific, Bremen, Germany). Raw delta values were converted to final using laboratory standards (lithium carbonate, $\delta^{13}C = -46.6‰$ and a deep seawater, $\delta^{13}C = +0.8‰$) calibrated against standards NBS-19 and L-SVEC.

CO$_2$ Assimilation

A microcosm-based approach was employed to assess the potential for inorganic carbon uptake *in situ* through the addition of $NaH^{13}CO_3$. *In situ* microcosms were performed between noon and 4 PM under full or partial sun. Samples were collected using a pre-sterilized spatula or forceps and ~500-mg was placed into pre-combusted (12 h, $450°C$) serum vials or sterile 6-well flat bottom cell culture plates (Fisher Scientific, Pittsburgh, PA, USA). Care was taken to maintain the structure of mats, filaments, and stromatolites. Samples were overlaid with spring water from the collected site and serum vials were capped with gas-tight black butyl rubber septa or plates were capped with provided lids. Assays were initiated by addition of $NaH^{13}CO_3$ (100 μM final concentration) (Cambridge Isotope Laboratories, Inc., Andover, MA, USA). All serum vial assays were performed in triplicate. For plate assays, $n = 3$ replicates were performed: each well served as half of a replicate, with the two halves combined following drying and prior to grinding/homogenization (described below).

We assessed the potential for photoautotrophic (light) and chemoautotrophic (dark) $NaH^{13}CO_3$ uptake. In addition, the contribution of Photosystem II (PSII)-independent anoxygenic photoassimilation of CO_2 was determined in assays amended to a final concentration of 10 μM DCMU (the PSII inhibitor, 3-(3,4-dichlorphenyl)-1,1-dimethylurea) (Sigma-Aldrich, St. Louis, MO, USA). Assays at Sites 1A−1C, 2, 3, and 4 were amended with DCMU. Due to sample limitation, assays at Site 1D (stromatolite) were not amended with DCMU. To assess CO_2 assimilation in the dark, vials ($n = 3$ replicates) or a plate ($n = 3$ replicates), were amended with $NaH^{13}CO_3$ and completely wrapped in aluminum foil. Assays were stopped by flash freezing vials or plates on dry ice. All vials and plates were stored at $-80°C$ until processed (described below). Reported values of ^{13}C-labeled DIC

FIGURE 1 | Map of Yellowstone with zoom in of GOPA showing sample locations and biofilms.
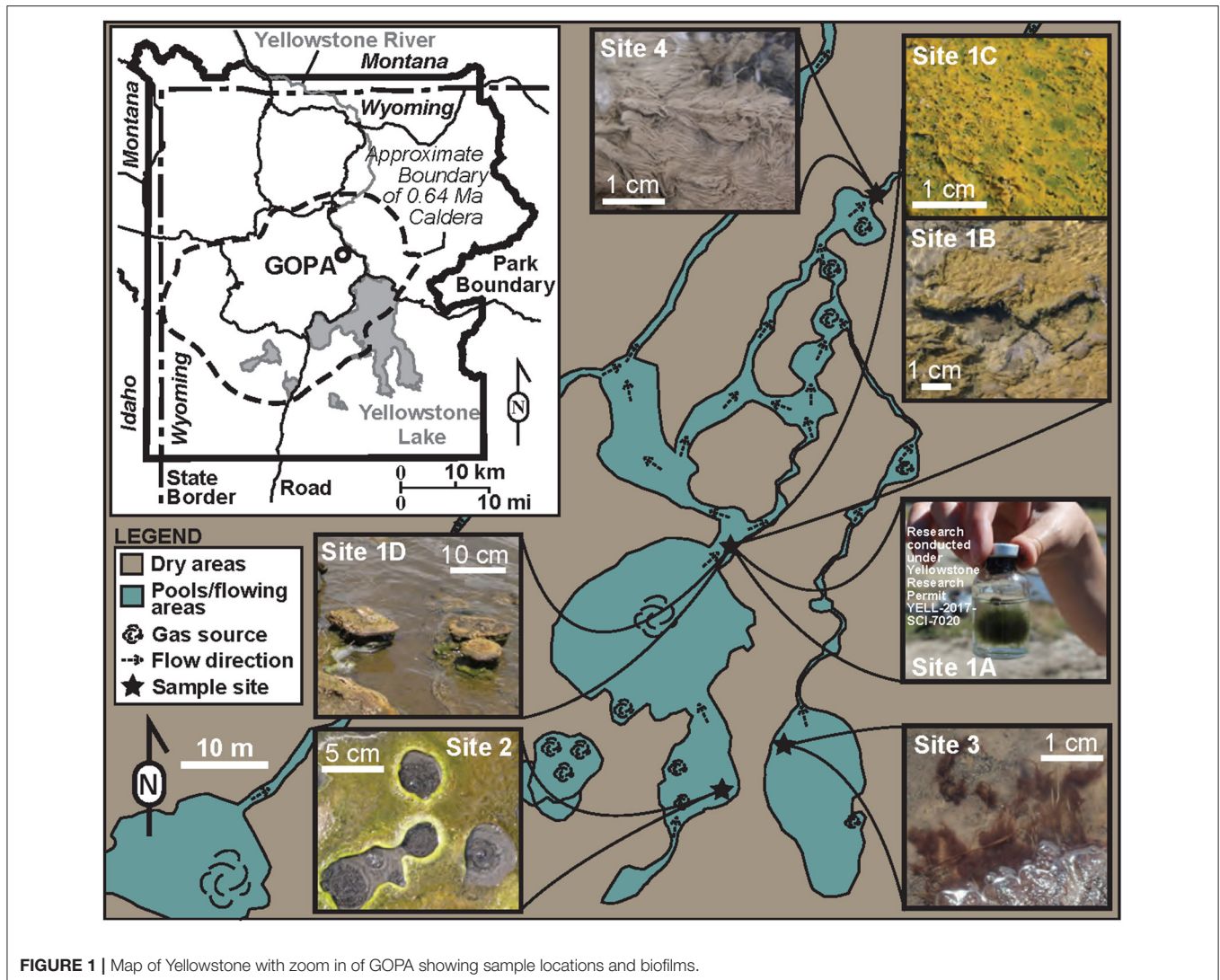
uptake (carbon fixation rates) reflect the difference in uptake between the biomass in the assays that received $NaH^{13}CO_3$ and the natural abundance biomass samples described below. For comparisons between mean ^{13}C uptake rates, a one-way ANOVA followed by *post-hoc* pairwise comparisons between treatments was conducted using a Turkey honest significant difference (HSD) within the R software package (R version 3.3.2). Mean rates with $p < 0.05$ were considered significantly different.

C and N Concentration and Stable Isotope Signals

Natural abundance samples were collected at the time of sampling and frozen until processed, except for the stromatolite sample. To minimize sampling impact, the stromatolite natural abundance sample were taken from Havig (2009), collected from approximately the same location in 2005 and 2006 and analyzed as described in Havig (2009). Assays were thawed and biomass was washed with HCl (1 M) to remove any extra ^{13}C-labeled DIC, triple washed with 18.2 MΩ/cm deionized

water, then dried (60°C for 3 days). Natural abundance samples were dried as described without the acid washing step used for assay biomass samples. Previous work has demonstrated that silica-saturated Yellowstone hydrothermal water sampled is undersaturated with respect to carbonate minerals, and that there was no effect from carbonate minerals on biomass carbon stable isotope values (Havig, 2009). Recent work has demonstrated intracellular precipitation of carbonate minerals by thermophilic cyanobacteria (e.g., Benzerara et al., 2014). However, these laboratory experiments were carried out under alkaline conditions hindering our ability to directly translate these affects to our samples from lower pH systems. Thus, we assume any effects of carbonate mineral precipitation on the carbon isotope signal to be negligible. Dried biomass was ground/homogenized with a cleaned mortar and pestle (ground with ethanol silica slurry, triple rinsed with 18.2 MΩ/cm deionized water, dried). Dried and ground samples for determination of C and N concentration and stable isotope signal were weighed and placed into tin boats, sealed,

and analyzed via a Costech Instruments Elemental Analyzer (EA) periphery connected to a Thermo Scientific Delta V Advantage Isotope Ratio Mass Spectrometer (IR-MS) at the Stable Isotope Geochemistry Lab in the Department of Geology at the University of Cincinnati, Cincinnati, OH, USA. Linearity corrections were made using NIST Standard 2710, and δ^{13}C values were calibrated using reference standards USGS-40 and USGS-41 and checked with a laboratory working standard (glycine). Total uptake of DIC was calculated using DIC numbers determined for the source water (described above). All stable isotope results are given in delta formation expressed as per mil (‰). Carbon stable isotopes are calculated as:

$$\delta^{13}C = [((R_a)_{sample}/(R_a)_{standard}) - 1] \times 10^3, \quad (1)$$

where R_a is the ^{13}C/^{12}C ratio of the sample or standard, and are reported vs. the Vienna Pee Dee Belemnite (VPDB) standard.

Precautions were taken to minimize cross contamination of natural abundance samples with incubation assays. Natural abundance samples were processed and analyzed in turn, prior to incubation assays. All laboratory processing and weighing equipment was cleaned with 80% ethanol between each sample. Standard checks and blanks were run within each analysis batch (49 samples and standards per batch) to check for memory effects or cross contamination of samples, with none detected.

Assimilation rates were calculated from the following parameters: Absolute isotopic stable carbon ratios were used to determine the difference between the total amount of ^{13}C in natural abundance samples and incubation assay replicates. The difference represents total mass of ^{13}C-labeled DIC taken up during incubations. Incubation duration times were recorded in the field. Using the organic carbon content, the uptake rate is then calculated from the total μg C taken up divided by the grams of organic C per gram of sediment, and that was divided by the number of hours the incubation was carried out over (typically ∼ 2 h).

DNA Extraction and Quantification

DNA was extracted from ∼250 mg of biomass using a DNeasy PowerSoil Kit (Qiagen, Carlsbad, CA, USA) according to the manufacturer's instructions. DNA was excreted from each replicate sample ($n = 3$) and the concentration of DNA was determined using a Qubit dsDNA HS Assay kit and a Qubit 3.0 Fluorometer (Invitrogen, Burlington, ON, Canada). The concentration of DNA in the replicates was within 5% for each sample. Equal volumes of each extraction was pooled and the concentration of the pooled extract was determined as described above. As a negative DNA extraction control, DNA was extracted from the filter used for the field blank water sample (described above). No DNA was detected in the control and sequencing failed to generate amplicons (see below for amplicon sequencing details).

Sequence Analysis

For archaeal and bacterial 16S rRNA gene sequencing, total DNA was submitted to the Center for Bioinformatics & Functional Genomics at Miami University (Oxford, OH, USA). Bacterial

and archaeal 16S rRNA gene sequences were targeted using the primers 515f and 806rB (Caporaso et al., 2012; Apprill et al., 2015). For eukaryotic 18S rRNA sequencing, total DNA was submitted to the Centre for Comparative Genomics and Evolutionary Bioinformatics (CGEB) at Dalhousie University (Halifax, Nova Scotia, Canada). Eukaryotic 18S rRNA sequences were targeted using the primers (E572F) and (E1009) (Comeau et al., 2011). Amplicons were sequenced using MiSeq Illumina 2 × 300 bp chemistry. Each sample was sequenced once. Post-sequence processing was performed within the mothur (ver. 1.39.3) sequence analysis platform (Schloss et al., 2009) following the MiSeq SOP (Kozich et al., 2013). Briefly, read pairs were assembled and resulting contigs with ambiguous bases were removed. Contigs were trimmed to include only the overlapping regions and unique sequences were aligned against a SILVA-based reference alignment and classified using a Bayesian classifier within mothur against the Silva (v128) reference taxonomy. Chimeras were identified in the aligned sequences using UCHIME (Edgar et al., 2011) with the Silva SEED database (v128) and removed from further analyses. Singletons were removed using the remove.rare function within mothur. Following removal of chimeras and singletons, sequences were binned into operational taxonomic units (OTUs) based on a sequence similarity of 97.0% for archaea and bacteria and 98% for eukarya using the OptiClust algorithm. Rarefaction was calculated within mothur and based on rarefaction analysis, >95% of the predicted 16S and 18S rRNA gene diversity was sampled at this depth of sequencing (data not shown). Differences in archaeal, bacterial, and eukaryotic community compositions were visualized using non-metric multi-dimensional scaling (NMDS) ordination with the R package Phyloseq (ver. 1.16.2; McMurdie and Holmes, 2013) using Bray-Curtis dissimilarities. Prior to ordination, relative abundance for each data set was normalized by the number of reads. Chao1 species richness estimates and Shannon diversity indices were calculated with Phyloseq. Results were visualized with the R packages Phyloseq and ampvis (Albertsen et al., 2015) (R version 3.2.4). Sequence data including raw reads, quality scores and mapping data have been deposited in the NCBI Sequence Read Archive (SRA) database with the BioProject number PRJNA395419.

RESULTS

Geochemistry and Morphology

We targeted a site at GOPA in which phototrophic filaments, mats and stromatolites grow within close proximity (Sites 1A–D) (**Figure 1**). Site 1 contains green filaments (1A), green and orange mats (1B and 1C, respectively), and stromatolites (1D), and had a pH 6.3 and a temperature of 48.4°C. Three nearby sites were also sampled which each contained a single type of microbial structure: An upstream hot spring that contained a green phototrophic mat (Site 2; **Figure 1**); purple phototrophic filaments from a nearby pool (Site 3; **Figure 1**); and gray chemotrophic filaments were collected from a site downstream (Site 4) (**Figure 1**). Site 2 had a pH of 6.1 and temperature of 45.1°C whereas Site 3 which had the lowest pH (3.9) and temperature (29.4°C) of our sample sites (**Table 1**). Site 4 had a

pH of 5.4 and the highest temperature (68.4°C) (**Table 1**). Sulfide ranged from 1.3 to 2.3 μM in the sample sites. Concentrations of Fe^{2+} ranged from 4.1 to 7.0 μM in Sites 1, 2, and 4, whereas Fe^{2+} concentration was 43.0 μM at Site 3. Dissolved silica concentrations ranged from 1.99 mM at Site 2 to 4.68 mM at Site 4 (**Table 1**). The DIC concentration was highest at Site 3 (7.91 mM), and was lowest at Site 4 (0.81 mM), with Sites 1 and 2 falling between those values (1.35 and 3.10 mM, respectively). DIC $\delta^{13}C$ values for the study sites were all close to zero, with Sites 1 and 2 having positive values (1.98 and 1.38‰, respectively) and Sites 3 and 4 having negative values (−2.52 and −0.76‰, respectively).

C and N Content and $\delta^{13}C$ Natural Abundance

The green filaments at Site 1A had the highest C (11.5%) and N (1.8%) content of all morphologies included in the study (**Table 2**). The green and orange mats from Sites 1B, 1C and Site 2 ranged in C from 2.6 to 8.3% and N from 0.3 to 1.1%. The carbon and nitrogen content of the stromatolite sample (1D) and the purple phototropic filaments (Site 3) were similar to the green and orange mats of Site 1, ranging from 3.0 to 4.8% C and from 0.4 to 0.6% N. The gray filaments from Site 4 had the lowest percent C and N of all samples, 1.8 and 0.2%, respectively. The natural abundance $\delta^{13}C$ values of the biomass ranged from −24.32‰ (Site 4 purple filaments) to −11.01‰ (Site 1A green

filaments) (**Table 2**). For mat samples, values ranged from −14.29 to −23.96‰ whereas the purple phototrophic filaments (Site 3) had $\delta^{13}C$ values of −24.32‰ compared to −11.01‰ for the green phototrophic filaments at Site 1 (1A) (**Table 2**). The gray filaments at Site 4 had a $\delta^{13}C$ value of −23.48‰. The stromatolite biomass (1D) had a $\delta^{13}C$ value of −13.90‰. Incubation assay % C and % N values for nearly all the sites were similar to those of the natural abundance samples, and most of the incubation assays with ^{13}C label added had $\delta^{13}C$ values more positive than the natural abundance samples (Table S1). The only exception was Site 3, where incubation assay carbon contents were higher than the natural abundance samples, and the Dark and DCMU treatments had $\delta^{13}C$ values indistinguishable from the natural abundance samples. The large range in carbon content is likely linked to the relative ages of samples collected, with organic carbon content inversely correlated to the amount of amorphous silica precipitate accumulated by the filaments (Havig, 2009; Havig et al., 2011). The similarity between natural abundance and Dark and DCMU incubation assays is linked to a lack of uptake of ^{13}C-labeled DIC (reported and discussed below).

Carbon Assimilation

A microcosm-based approach was employed to assess the potential for inorganic carbon uptake *in situ* across morphologies in the GOPA area through the addition of $NaH^{13}CO_3$. We assessed light-dependent and light-independent inorganic

TABLE 1 | Aqueous geochemistry of sites at the Greater Obsidian Pool Area (GOPA) where microcosms were performed.

Site	pH	T (°C)	Conductivity (μS/cm)	SiO₂ (mM)	Cl⁻ (mM)	SO₄²⁻ (mM)	DIC (mM)	δ¹³C_DIC (‰)	Na⁺ (mM)	K⁺ (mM)	Ca²⁺ (mM)	Mg²⁺ (mM)	Sulfide (μM)	Fe²⁺ (μM)
Site 1	6.28	48.4	1,625	2.31	8.24	2.70	1.35	1.98	12.81	1.12	0.15	0.03	2.25	6.45
Site 2	6.07	45.1	762	*1.99*	1.98	1.33	3.10	1.38	4.04	0.73	0.62	0.36	2.20	4.12
Site 3	3.87	29.4	867	2.04	1.48	3.11	7.91	−2.52	3.86	0.73	0.55	0.40	1.28	42.97
Site 4	5.44	68.4	1,633	4.68	7.85	2.96	0.81	−0.76	12.50	1.05	0.14	0.04	1.69	7.04

Sample locations are indicated in **Figure 1**. *SiO₂, sulfide, and Fe²⁺ measured via spectrophotometry. Dissolved inorganic carbon (DIC) measured via IR-MS. Cl⁻ and SO₄²⁻ measured via IC Na⁺, K⁺, Ca²⁺, and Mg²⁺ measured via ICP-MS. Site2 dissolved silica(SiO₂) analysis from 2017. DIC δ¹³ values (δ¹³C_DIC) reported vs. VPDB. Value in italics from Havig (2009).*

TABLE 2 | Carbon assimilation rates and δ¹³C natural abundance.

Site	Biofilm Description		Carbon uptake rates (μg C/g biomass C/hr)				C (%)	N (%)	δ¹³C (‰)
			Total C	Oxygenic Photo.[a]	Anoxygenic Photo.[b]	Chemoautotrophy			
Site 1A	Filaments	P	300.6 (±32.4)	261.6 (±32.6)	27.2 (±3.4)	11.8 (±0.2)	11.45	1.80	−11.01
Site 1B	Mat	P	134.0 (±42.2)	109.7 (±42.4)	10.6 (±4.2)	13.6 (±1.5)	3.25	0.36	−23.96
Site 1C	Mat	P	78.2 (±19.4)	62.3 (±19.5)	5.5 (±2.7)	10.3 (±2.3)	2.61	0.28	−21.97
Site 1D	Stromatolite	P	39.6 (±4.0)	38.2 (±4.0)	nd	1.4 (±0.6)	*4.77*	*0.60*	*−13.90*
Site 2	Mat	P	39.5 (±20.0)	28.4 (±20.0)	nr	11.1 (±0.4)	8.26	1.05	−14.29
Site 3	Filaments	P	46.7 (±10.6)	45.8 (±10.6)	0.9 (±20.0)	0	3.02	0.36	−24.32
Site 4	Filaments	C	18.1 (±1.6)	N/A	N/A	18.1 (±1.6)	1.75	0.17	−23.48

Sample locations are indicated in **Figure 1**. *DIC δ¹³C values are provided in* **Table 1**.
[a]*Oxygenic photoautotrophic carbon uptake calculated from light treatment carbon uptake minus DCMU or dark treatment carbon uptake.*
[b]*Anoxygenic photoautotrophic carbon uptake calculated from DCMU treatment uptake minus dark treatment carbon uptake. C, N, and δ¹³C reported for natural abundance samples. P, phototrophic; C, chemotrophic; nd, not determined; nr, null result; N/A, not applicable. δ¹³C values reported vs. VPBD. Site 1D % C, % N, and δ¹³C values from Havig (2009). Value in italics from Havig (2009).*

carbon uptake in green mats, orange mats, green filaments and stromatolites in Sites 1 and 2 as well as the purple filaments from Ssite 3, and gray filaments from Site 4. The highest rates of inorganic carbon uptake we observed were in the green filaments from Site 1 (1A) when exposed to light (300.6 μg C/g C$_{biomass}$/hr) (**Table 2**; **Figure 2**). We also observed light dependent inorganic carbon uptake in the green mat (Site 1B) and orange mat from site 1 (134.0 and 78.2 μg C/g C$_{biomass}$/hr, respectively) (**Table 2**; **Figure 2**). Light-dependent inorganic carbon uptake rates in the stromatolite (Site 1D), Site 2 green mat, and Site 3 purple filaments were lower (39.6, 39.5, and 46.7 μg C/g C$_{biomass}$/hr, respectively) (**Table 2**; **Figure 2**).

The potential for light-independent primary productivity (chemolithoautotrophy) was observed in all sites except the purple filaments of Site 3. In all samples except the gray filaments at Site 4, inorganic carbon uptake rates were higher in the light compared to those in the dark. At Site 4, no significant difference was observed between NaH^{13}CO$_3$ uptake in the light vs. dark (**Table 2**; **Figure 2**) which suggests only chemoautotrophic primary productivity occurs in the gray filaments. No incorporation of NaH^{13}CO$_3$ in the dark was observed in the filaments from Site 3 (**Table 2**; **Figure 3**). In the Sites 1 and 2, dark primary productivity ranged from 1.4 μg C/g C$_{biomass}$/hr in the stromatolite to 10.3–13.6 μg C/g C$_{biomass}$/hr in the orange and green mats, respectively (**Table 2**; **Figure 2**).

A subset of *in situ* microcosms were performed in the presence of DCMU to assess the potential for PSII-independent (anoxygenic) photosynthesis. Incorporation of NaH^{13}CO$_3$ was observed in the presence of DCMU in the green filaments, green mat, and orange mat from Site 1 (1A, 1B, and 1C), with anoxygenic photosynthesis (calculated from DCMU treatment minus dark treatment uptake values) contributing from 5.5 to 27.2 μg C/g C$_{biomass}$/hr (**Table 2**; **Figure 2**). Similar to the light-dependent microcosms, rates of anoxygenic photosynthesis NaH^{13}CO$_3$ uptake were highest in the green filaments at Site 1 (1A) (**Figure 2**). Based on the lack of evidence for light-independent primary productivity, our observations indicate carbon fixation in the purple filaments occurs through the activity of oxygenic phototrophs. Rates of NaH^{13}CO$_3$ incorporation at Site 4 in assays amended with DCMU were less than the light and dark treatments, suggesting potential inhibition of chemoautotrophic carbon uptake.
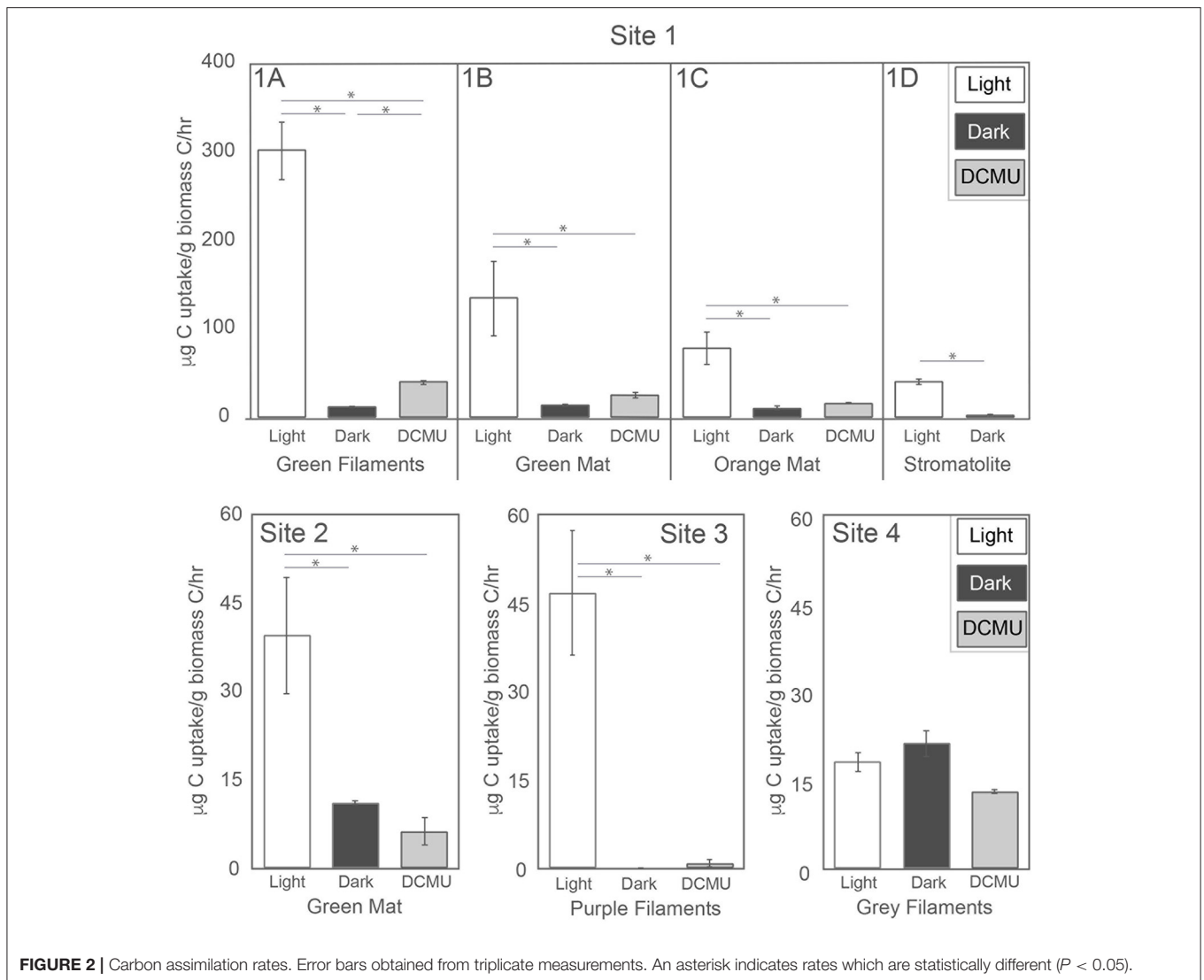
Community Composition and Diversity
Following quality control, merging of contigs, and removal of chimeras and singletons, we recovered 334,832 16S rRNA sequences with an average length of 253 bp and 283,868 18S rRNA sequences with an average length of 440 bp (Table S2). The libraries ranged in size from ~13,000 to 118,904 total sequences following quality control. At a sequence identity of 97%, we recovered 263 OTUs affiliated with archaea and 10,353 OTUs affiliated with bacteria. At a sequence identity of 98%, we recovered 3,276 18S rRNA OTUs. Species richness, estimated using Chao1, was highest for bacterial OTUs in the green mat from Site 1 whereas archaeal Chao1 richness was highest in the gray filaments from Site 4 (Figure S2). The highest estimated Chao1 richness for the eukaryotic libraries was observed in

the purple filaments from Site 3 (Figure S2). The stromatolite from Site 1 had the lowest estimated richness. For bacteria, the Shannon diversity index was highest in the mat samples from Site 1 and 2 as well as the purple filaments from Site 3. Bacterial diversity was lowest in the gray filaments from Site 4. The Shannon diversity of archaeal OTUs was highest in the green mat from Site 2. Values for the Site 1 samples were similar while archaeal diversity was the lowest in the purple filaments from Site 3. The highest Shannon diversity for the eukaryotic libraries was observed in the orange mat and stromatolite samples from Site 1. The green filaments at Site 1 and green mat from Site 3 had the lowest values of Shannon diversity in the samples. An NMDS analysis of Bray–Curtis similarities in the bacterial, archaeal, and eukaryotic data indicate the communities from Site 1 and Site 2 are more closely related than those in the purple filaments from Site 3 and the gray filaments from Site 4 (Figure S3). Microbial communities from Site 3 and Site 4 are distinct. These data are consistent with similarity in physicochemical characteristics of Site 1 and Site 2 compared to Site 3 (acidic pH, lower temperature) and 4 (higher temperature).
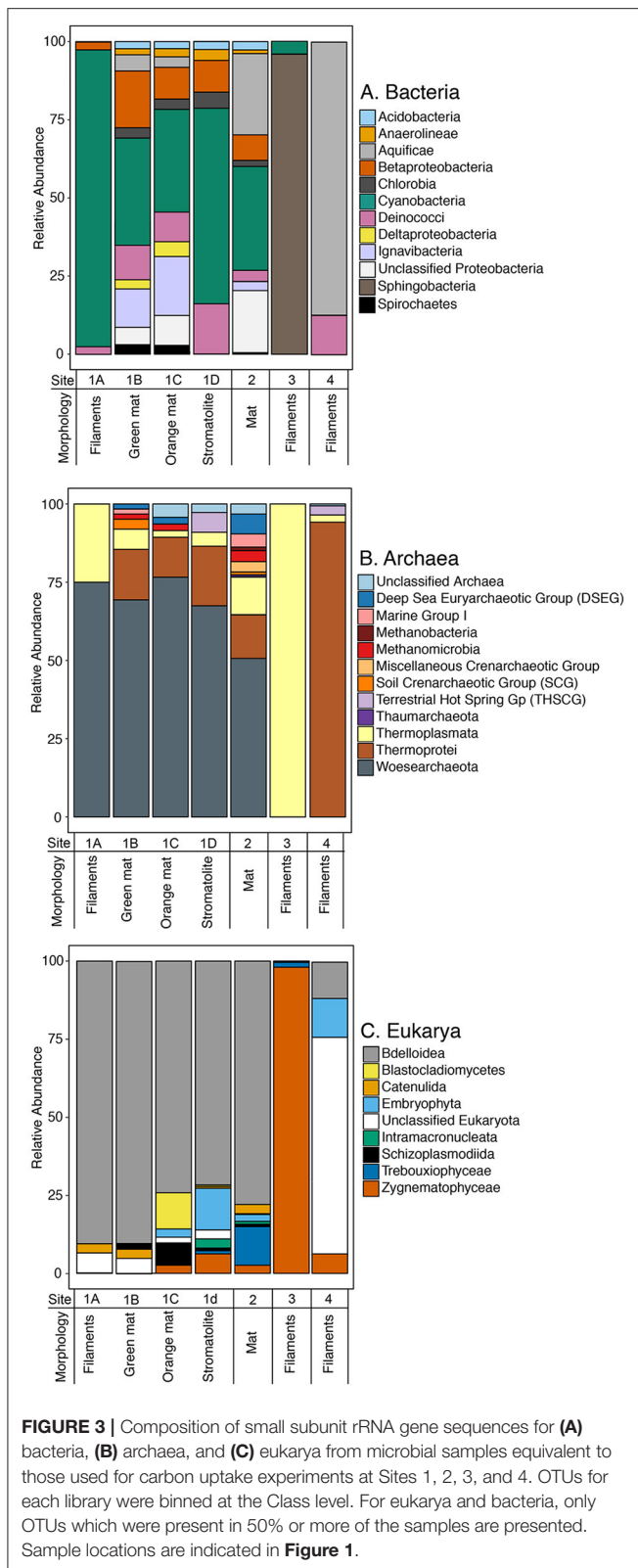
Bacteria
The majority of bacterial OTUs recovered were affiliated with Cyanobacteria, Betaproteobacteria, Deinococci, Alphaproteobacteria, Ignavibacteria, and Aquificae (**Figure 3A**; Figure S1A). Consistent with evidence for light-dependent primary productivity in the majority of the samples (**Figure 3**, **Table 2**), OTUs affiliated with Cyanobacteria were abundant in the mats, filaments and stromatolite in Sites 1 and 2. In particular, OTUs affiliated with Cyanobacteria accounted for > 95% of the total sequences in the green filaments in Site 1A, > 65% of the total sequences in the stromatolite, and ~30% of the total sequences in Sites 1B (green mat), 1C (orange mat), and Site 2 (green mat) (**Figure 3A**). Cyanobacterial OTUs affiliated with *Thermosynechococcus* spp were abundant in the green filaments and green and orange mats in Site 1 (1A, 1B, and 1C) and comprised a small fraction of the bacterial OTUs recovered from the purple filaments (Site 3). In particular, a single OTU assigned to *Thermosynechococcus* was recovered from Site 1 samples, accounting for up to 10% of the total sequences. *Thermosynechococcus* spp. are common oxygenic phototrophs in hot springs with moderate temperatures (Everroad et al., 2012). Consistent with previous studies of stromatolites in GOPA (Berelson et al., 2011; Pepe-Ranney et al., 2012), OTUs affiliated with mat-forming *Chlorogloeopsis* spp. and filamentous *Fischerella* spp. were recovered from the stromatolite sample (Site 1D). A single OTU of *Chlorogloeopsis* accounted for ~10% of the cyanobacterial sequence recovered from the stromatolite while smaller numbers of this OTU were recovered from the other Site 1 samples and Site 2. In YNP, both *Chlorogloeopsis* spp. and *Fischerella* spp. have been observed to predominate in lower pH springs where *Synechococcus* is absent (Castenholz, 1977, 1978). OTUs affiliated with unicellular *Gloeocapsa* spp. and the filamentous cyanobacteria *Arthronema* and *Leptolyngbya* spp. were also recovered from the samples in Site 1 and Site 2. Single OTUs assigned to *Gloeocapsa* and *Leptolyngbya* accounted for 30% of the total sequences in the green mat from Site 1. The

FIGURE 2 | Carbon assimilation rates. Error bars obtained from triplicate measurements. An asterisk indicates rates which are statistically different ($P < 0.05$).

same OTU was recovered from the green filaments at Site 1 but in much lower abundance (~3%). Sequences affiliated with *Leptolyngbya* have been recovered from coniform structures in YNP (Reyes et al., 2013). We also recovered OTUs affiliated with phototrophic members of the Chlorobi and filamentous anoxygenic phototrophs (FAPs) of the phylum Chloroflexi (*Roseiflexus* spp.). Sequences affiliated with these are commonly observed in hot spring phototrophic mats (Klatt et al., 2011; Tank et al., 2017) and could contribute to light-dependent inorganic carbon uptake in the presence of DCMU (anoxygenic photosynthesis) observed in Sites 1A, 1B, 1C and Site 2 (**Figure 3**; **Table 2**).

OTUs affiliated with Sphingobacteria accounted for the majority of sequences (~97%) recovered from the purple filaments in Site 3 (**Figure 3A**). Sphingobacteria have been recovered from geothermal springs that are more alkaline (pH range of 7.7–9.5) than that found at Site 3 (pH 3.9) (Tekere et al., 2011; Tobler and Benning, 2011). OTUs affiliated with Aquificae, a hyperthermophilic chemoautotroph found in both

terrestrial hot springs as well as hydrothermal vents (Hügler et al., 2007), were recovered from all sites and were abundant in Site 4 (~94% relative abundance) (**Figure 3A**). A single Aquificae OTU in Site 4 accounted for ~75% of the total sequences recovered from the gray filaments. The same OTU was recovered from Site 1 and Site 2. The majority of Aquificae OTUs recovered, including the abundant OTU from Site 4, were most closely related to *Sulfurihydrogenibium* spp., which are common in flowing hot springs where they form filamentous masses that precipitate iron and sulfur minerals (Reysenbach et al., 2005). OTUs affiliated with Ignavibacteria were recovered from the green and orange mats in Site 1 (1B and 1C) and the green mat in Site 2 (**Figure 2A**). The Ignavibacteria OTUs were most closely related to *Ignavibacteriales* assigned to the Families SR-FBR-L83 and IheB3-7. Neither have cultured representatives but a close relative of SR-FBR-L83 is a moderate thermophile and facultative anaerobe that can respire diverse electron acceptors, e.g., Fe(III), NO_2^-, and AsO_4^{3-} (Podosokorskaya et al., 2013). OTUs affiliated with Deinococci (*Thermus* and *Meiothermus*

FIGURE 3 | Composition of small subunit rRNA gene sequences for **(A)** bacteria, **(B)** archaea, and **(C)** eukarya from microbial samples equivalent to those used for carbon uptake experiments at Sites 1, 2, 3, and 4. OTUs for each library were binned at the Class level. For eukarya and bacteria, only OTUs which were present in 50% or more of the samples are presented. Sample locations are indicated in **Figure 1**.

spp.) and Betaproteobacteria were recovered from all of the samples except the purple filaments of Site 3. The same *Thermus* OTU was recovered from the stromatolite and gray filament

samples, accounting for ∼5% of the sequences whereas an OTU assigned to *Meiothermus* accounted for ∼5–6% of the sequences in the orange and green mats from Site 1. Deinococci are common in hot springs that range in pH 6.0–9.0 and temperature ranges from 45 to 57°C (Ferreira et al., 1997) while sequences affiliated with diverse Betaproteobactera have been recovered from hot springs ranging in temperature from 29 to 57 °C and pH ranges from acidic to alkaline (pH 2.7–8.0) (Kanokratana et al., 2004; Jiménez et al., 2012; Coman et al., 2013).

Archaea

The majority of archaeal OTUs affiliated were assigned to Thermoprotei or Woesearchaeota (**Figure 3B**; Figure S1B). Woesearchaeota (formerly in the Euryarchaeota DHVEG-6 cluster) (Castelle et al., 2015) OTUs were most abundant in samples from Sites 1 and 2, accounting for 50–75% of the total sequences recovered from these samples (**Figure 3B**). Sequences affiliated with Woesearchaeota have been recovered from diverse environments ranging from surface waters of oligotrophic high-altitude lakes (Ortiz-Alvarez and Casamayor, 2016), stratified microbial mats (Saghaï et al., 2017), sediments, plankton and hydrothermal vents (Robertson et al., 2009; Pachiadaki et al., 2011), and hot springs (Kan et al., 2011). A single Woesearchaeota OTU accounted for 45–50% of the sequences recovered from the green and orange mats from Site 1. OTUs affiliated with Thermoplasmata, typically found in acidic environments, hot springs, and acid main drainage sites with pH as low as 3.2 and temperatures as high as 84°C (Song et al., 2013), were abundant in Site 3 (∼99%) with a Thermoplasmata OTU accounting for >41% of the total sequences. The majority of OTUs in Site 4 (>96%) were affiliated with Thermoprotei including 2 OTUs affiliated with *Acidilobus* spp. and an OTU affiliated with *Sulfolobus* spp. which together accounted for ∼70% of the total sequences. Sequences affiliated with chemolithoautotrophic Thermoprotei (i.e., *Acidilobus* spp.) as well as the sulfur oxidizing *Sulfolobus* spp. are commonly recovered from acidic hot springs, mud pots, and hydrothermal marine environments that range from 65 to 100°C (Brock et al., 1972; Garrity et al., 2001). Small numbers of OTUs affiliated with Deep Sea Euryarchaeotic Group, Terrestrial Hot Spring Gp, Miscellaneous Crenarchaeotic Group, Marine Group I, and two classes of methanogens, Methanobacteria and Methanomicrobia were also recovered from the majority of the samples (**Figure 3B**).

Eukarya

The majority of eukaryotic OTUs recovered were affiliated with Bdelloidea (Rotifers) and Zygnematophyceae (green algae) (**Figure 3C**; Figure S1C). OTUs affiliated with Bdelloidea were abundant in the Site 1 and Site 2 samples. Bdelloidea have been found to inhabit hot springs at temperatures up to ∼45°C (McDermott and Skorupa, 2011) and thus they could be active under the conditions in Sites 1 and 2. However, Bdelloidea can undergo cryptobiosis, a stage of dormancy, in response to extreme environmental conditions (Pejler, 1995). This could explain the recovery of 18S rRNA gene sequences affiliated with Bdelloidea from these sites, especially Site 4

(68.4°C), where the temperature exceeds their maximum known temperature tolerance (~45°C). In the purple filaments from Site 3, OTUs affiliated with the green alga Zygnematophyceae (*Zygogonium*) accounted for the majority of sequences recovered (~98%). Mats of *Zygogonium* filaments are common in and near acidic geothermal springs with temperatures below 40°C (Lynn and Brock, 1969) (Site 3: pH of 3.87, 29.4°C). The recovery of abundant 18S rRNA OTUs affiliated with Zygnematophyceae from Site 3 suggests the light-dependent inorganic carbon uptake observed can be attributed to this eukaryotic oxygenic phototroph. Consistent with previous characterization of stromatolites in GOPA (Berelson et al., 2011; Pepe-Ranney et al., 2012), we also recovered a small number of OTUs (10 OTUs) affiliated with diatoms from our stromatolite samples (Site 1D).

DISCUSSION

Carbon Uptake and Microbial Community Morphology

The rock record preserves microbially generated structures, including filaments, mats, and stromatolites. Among these, stromatolites are the most often preserved microbial structures recovered from ancient rocks. Stromatolites have been found in rocks dating back to 3.5 Ga (e.g., van Kranendonk et al., 2008; Wacey, 2010), and putative stromatolite-like features before 3.7 Ga (Nutman et al., 2016). In general, stromatolites are assumed to be generated at least in part by the activity of phototrophic microbial communities in shallow water environments (Riding, 2011; Stal, 2012). Microbial mat and filament features are much less common in the rock record, and when present are usually found as microfossils in chert (e.g., Buick, 1990; Schopf, 1993; Schieber, 1998; Tice and Lowe, 2004; Noffke et al., 2006). The dominant architects of modern microbial mats and filaments can be photoautotrophs or chemoautotrophs, confounding the interpretation of these structures in the rock record. Preferential preservation of stromatolites over mats and filaments may generate an inherent bias toward assuming stromatolites as a major driving force in productivity and generating oxygen. In the present study, we sought to constrain the role of environmental factors to examine community composition and productivity in predominantly phototrophic microbial structures commonly encountered in the rock record. Specifically, we targeted a geothermal feature in the Mud Volcano Area of Yellowstone National Park where the same pool (Site 1, **Figure 1**) contains a natural succession of filaments, mats, and stromatolites. Our study also includes samples of phototrophic mat, eukaryotic phototrophic filaments, and chemotropic filaments from nearby hot springs to help constrain ambiguity in interpreting these structures in the rock record.

Primary Productivity in Filaments, Mats, and Stromatolites
Key Differences in Carbon Uptake and Potential Oxygen Production by Structures in Site 1
At Site 1, four predominantly cyanobacterial phototrophic microbial communities were assessed for carbon uptake rates,

a filamentous community (Site 1A), two mat communities (a green mat at Site 1B and an orange-green mat at Site 1C), and a stromatolite community (Site 1D) (**Figure 1**). Of these, the filamentous community at Site 1A exhibited the greatest rate of carbon uptake of 300.6 μg C/g $C_{biomass}$ /hr. The treatment conducted in the dark for quantifying chemotrophic carbon fixation for Site 1A had an uptake rate of 11.8 μg C/g $C_{biomass}$ /hr, and the treatment quantifying anoxygenic photosynthesis yielded 27.2 μg C/g $C_{biomass}$/hr above that of the chemotrophic background (i.e., Dark subtracted from DCMU). From this, we calculate oxygenic photosynthesis at Site 1A accounts for ~83% of carbon fixation by the microbial community, or 261.5 μg C/g $C_{biomass}$/hr. Based on the carbon fixation reaction of oxygenic photosynthesis (CO_2 + H_2O → CH_2O + O_2), the filament community is generating 21.8 μmol O_2/g $C_{biomass}$/hr.

Two visually and spatially distinct subaqueous mat communities at Site 1 (Site 1B green mat and Site 1C orange-green mat, **Figure 1**) yielded lower uptake rates than the Site 1A filaments (**Table 2**). Of the mat sites, the Site 1B green mat exhibited a higher overall carbon uptake rate than the Site 1C orange-green mat, with a total carbon uptake rate of 134.0 μg C/g $C_{biomass}$/hr from a combination of oxygenic photosynthetic carbon uptake (109.4 μg C/g $C_{biomass}$/hr), anoxygenic photosynthetic carbon uptake (10.6 μg C/g $C_{biomass}$/hr) and chemotrophic carbon uptake (13.6 μg C/g $C_{biomass}$/hr). The Site 1C orange-green mat had an overall carbon uptake rate of 78.2 μg C/g $C_{biomass}$ /hr, from a combination of oxygenic photosynthesis (62.3 μg C/g $C_{biomass}$ /hr), anoxygenic photosynthesis (5.5 μg C/g $C_{biomass}$/hr), and chemotrophic (10.3 μg C/g $C_{biomass}$/hr) carbon uptake. These values equate to oxygen production of 9.1 μmol O_2/g $C_{biomass}$/hr for the Site 1B green mat and 5.2 μmol O_2/g $C_{biomass}$/hr for the Site 1C orange-green mat. The stromatolite community (Site 1D) had the lowest overall carbon uptake rates measured from Site 1, with a total uptake rate of 39.6 μg C/g $C_{biomass}$/hr, and a chemotrophic uptake rate of 1.4 μg C/g $C_{biomass}$/hr (anoxygenic photosynthesis was not quantified due to sample size limitations).

The amount of carbon uptake attributed to anoxygenic photosynthesis for Sites 1A, 1B, and 1C ranged from 7.1 to 9.1% of total carbon uptake. From these data, if we assume an average value (~8%) of total carbon uptake attributed to anoxygenic photosynthesis for the stromatolite community, this activity would account for 3.2 μg C/g $C_{biomass}$/hr, leaving 35.0 μg C/g $C_{biomass}$/hr attributed to the activity of oxygenic photosynthesis. From this, we estimate oxygen production by the stromatolite community at 2.9 μmol O_2/g $C_{biomass}$/hr. This value is 55.7–31.9% of the O_2 production by the mats, and nearly an order of magnitude lower than the filaments. Our results suggest ancient phototrophic filamentous and mat communities could have generated more O_2 per unit biomass than stromatolites.

Because methods employed to determine carbon fixation rates vary (^{13}C vs. [14]C, normalization) and our O_2 production rates are calculated from inorganic carbon uptake, it is difficult to compare to studies reporting primary productivity in hot springs which are host to photoautotrophs. The topography of mats, filaments, and stromatolites further complicates the issue (Bauld et al., 1979). Values of 156 mmol of O_2 dm^{3-1} h^{-1} have been report for oxygen production in phototrophic mats in Yellowstone National Park

(Octopus Spring) (Revsbach and Ward, 1984). Considering our samples are cm scale, our values from the phototrophic mats are consistent. Filaments in thermal spring in Mount Lassen National Park produced 0.33 to > 8 g of O_2 m^{2-1} (Stockner, 1968), which is again consistent with our observations for the phototrophic filaments in this study. In enrichment cultures of cyanobacteria that from conical stromatolites in YNP, oxygen production rates of ~1.5 nmol O_2 ml^{-1} were observed (Bosak et al., 2012). Ignoring biomass, we assume this equates to 90 nmol of O_2 hr^{-1} which is less than we estimate for our stromatolite sample. In mildly acidic hot springs in YNP, rates of inorganic carbon uptake by predominantly phototrophic communities (presumably mats and filaments) ranged from below 0.001 µg C hr^{-1} to ~0.5 µg C hr^{-1} (Fecteau, 2016) and in phototrophic mats in YNP, rates of inorganic carbon uptake ranged from less than 0.1 µg C g N^{-1} hr^{-1} to 157 µg C g N^{-1} hr^{-1} (Boyd et al., 2012). These studies are consistent with our observations for mats and filaments.

Chemoautotrophic vs. Photoautotrophic Rates of Primary Productivity Across Varying Geochemistry

For comparison of the microbial communities at Site 1, three other sites were sampled and carbon uptake experiments conducted. Site 2 had a temperature (45.1°C) and pH (6.1) similar to Site 1, and had a subaerial photosynthetic mat growing at the air-water interface (**Figure 1**) with a microbial community structure similar to those at Site 1 (**Figure 2**). Site 3 was a nearby pool that was cooler (29.4°C) and had a lower pH (3.9). The purple filaments at Site 3 were comprised of sequences affiliated eukaryotic phototrophs (**Figures 1**, **2**). Site 4 was located downstream of a hydrothermal source in the confluence outflow of Sites 1 and 3. Site 4 had a higher temperature (68.4°C) and slightly lower pH (5.4) than Site 1 and a predominantly bacterial chemotrophic filamentous microbial community present (**Figures 1**, **2**).

At Site 2, the photosynthetic mat had an overall carbon uptake rate of 39.5 µg C/g $C_{biomass}$/hr, with 28.4 µg C/g $C_{biomass}$ C/hr attributed to uptake by oxygenic photosynthesis and 11.1 µg C/g $C_{biomass}$/hr to chemotrophic carbon uptake (anoxygenic photosynthesis uptake experiments yielded a null result). From the total oxygenic photosynthesis uptake rate, conversion to O_2 production yields a rate of 2.4 µmol O_2/g $C_{biomass}$/hr, similar to those observed for the stromatolite sample (Site 1D).

The predominantly eukaryotic photosynthetic filaments from Site 3 had an overall carbon uptake rate of 46.7 µg C/g $C_{biomass}$/hr, with 0.9 µg C/g $C_{biomass}$/hr attributed to anoxygenic photosynthesis (as determined by the DCMU treatments) and no carbon uptake attributed to chemoautotrophy (dark treatments), giving an oxygenic photosynthesis carbon uptake rate of 45.8 µg C/g $C_{biomass}$/hr. Converting the carbon uptake attributed to oxygenic photosynthesis to O_2 production rates yields a rate of 3.8 µmol O_2/g $C_{biomass}$/hr, similar to the Site 1D stromatolites.

Site 4 contained predominantly bacterial chemoautotrophic filaments that had an overall carbon uptake rate of 18.1 µg C/g $C_{biomass}$/hr. Incubating the filaments in the dark yielded a carbon uptake rate of 21.3 µg C/g $C_{biomass}$/hr, similar to the light incubation values, showing no significant difference between light-dependent and light-independent carbon uptake

(**Figure 2**). These uptake rates are consistent with uptake rates of 0.1 µg C g N^{-1} hr^{-1} to 11 µg C g N^{-1} hr^{-1} reported for chemotrophic microbial communities in other YNP hot springs (Boyd et al., 2012). Treatment with DCMU yielded lower carbon uptake rates (13.1 µg C/g $C_{biomass}$/hr) (**Figure 2**). Because there was no difference in carbon uptake rates between the light and dark treatment (and phototrophs were not recovered; **Figure 3**), the decreased carbon uptake rates in the presence of DCMU suggests DCMU may inhibit chemoautotrophy. DCMU inhibits photosystem II (required for oxygenic photosynthesis) thus amendment with DCMU should represent the contribution of photosystem II-independent anoxygenic photoassimilation of inorganic carbon as well as chemoautotrophic carbon fixation. If chemoautotrophy is inhibited by DCMU addition, our rates of anoxygenic photosynthesis (determined by subtracting the DCMU treatment rate from the dark treatment rate) may represent an underestimation.
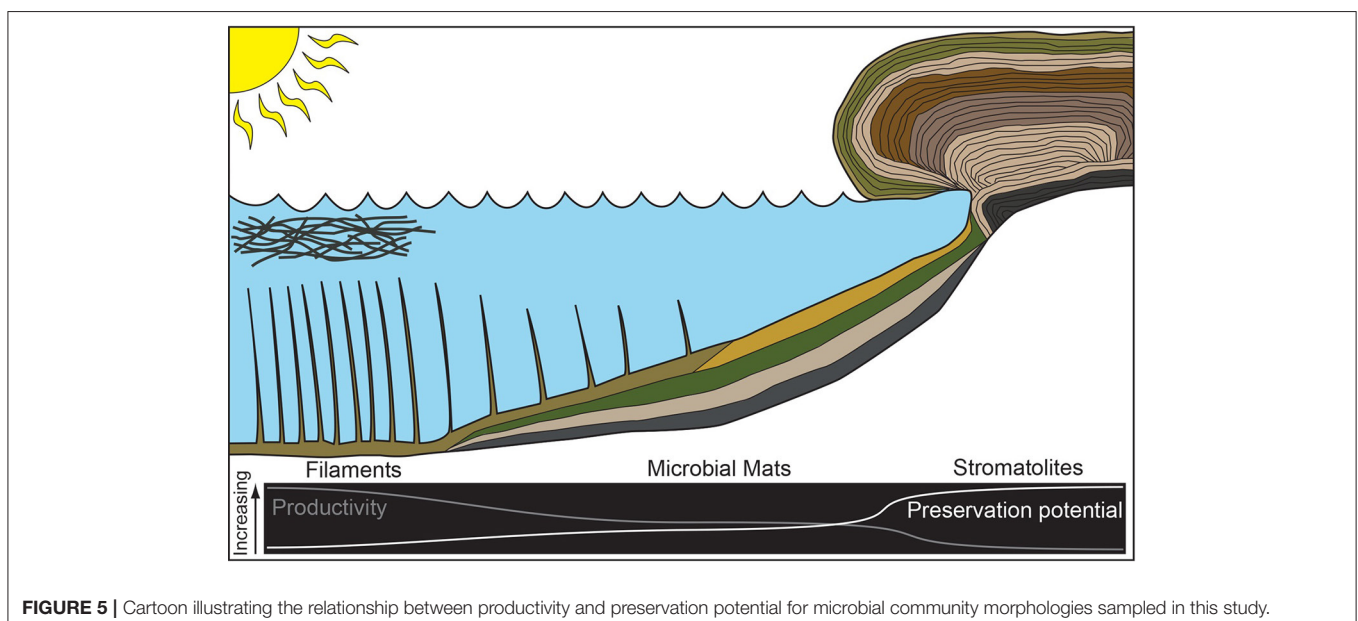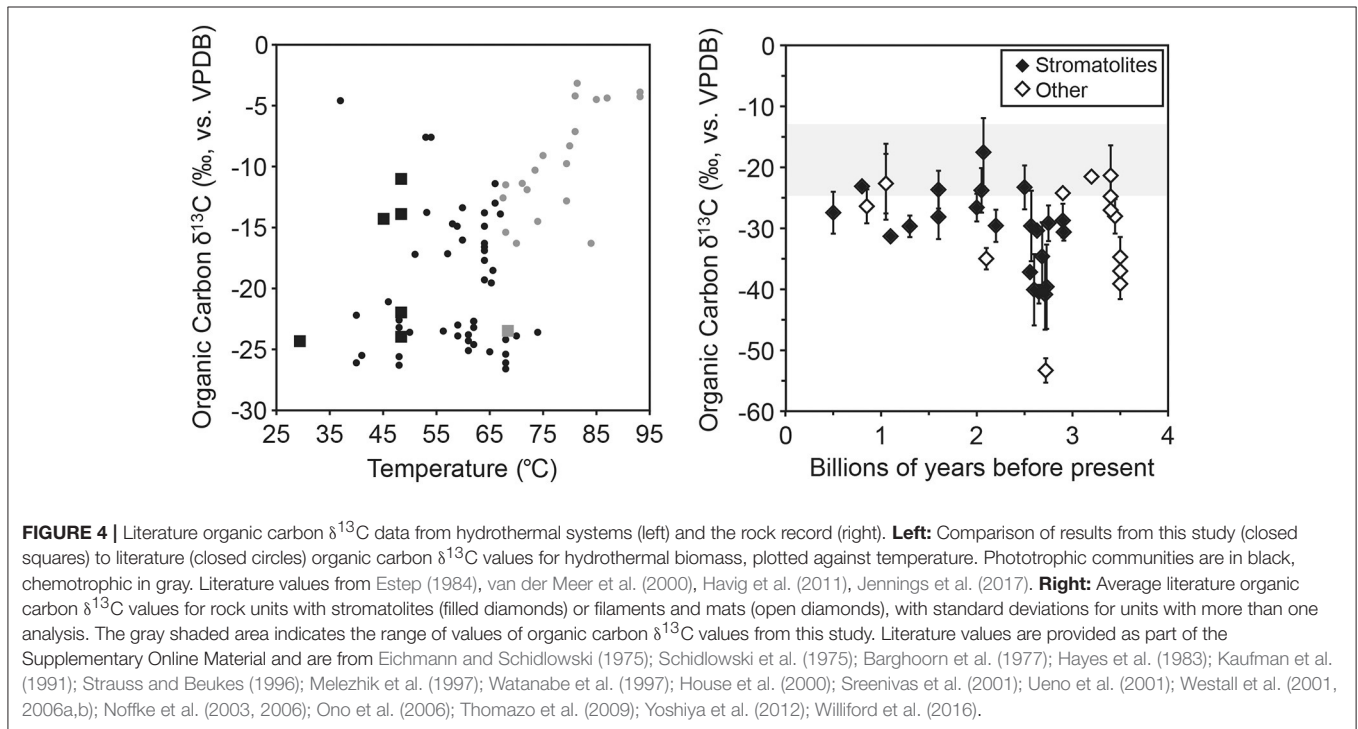
In our study, light-dependent carbon uptake rates by the stromatolite exceeded carbon uptake of the chemotrophic filaments exposed to light (Site 4). Considering the majority of carbon fixation in stromatolites is light-dependent (39.6 µg C/g $C_{biomass}$/hr), during daylight hours, the stromatolite has the potential to exceed carbon uptake of chemotrophic filaments ~2-fold. However, presumably chemoautotrophs fix carbon regardless of light cycle. In our study, rates of light-independent carbon fixation for the gray filaments far exceeded the stromatolite (21.3 µg C/g $C_{biomass}$/hr compared to 1.4 3 µg C/g $C_{biomass}$/hr). As a result, the chemotrophic filaments examined in this study have the potential to fix at least as much carbon as the stromatolite over a 24 h period. The observation that chemoautotrophy contributes to primary productivity in this stromatolite community where photoautotrophs appear abundant is consistent with recent observations of chemoautotrophy in shallow-(sea)water hydrothermal systems (Gomez-Saez et al., 2017) as well as other studies in YNP (Boyd et al., 2012; Fecteau, 2016); however, no cyanobacteria were recovered from the shallow vent system. Regardless, our data underscore the need for more studies considering the contribution of both chemo- and photoautotrophic communities to microbial structures and resulting signals recorded in the rock record.

Modern and Rock Record Biomass

We compiled examples of literature values for organic carbon $\delta^{13}C$ of biomass from hydrothermal filaments, mats, and stromatolites, including chemoautotrophic and photoautotrophic communities. These values ranged from −26.6 to −3.2‰, bracketing the range of −24.3 to −11.0‰ observed in this study (**Figure 4**). Previous work in hydrothermal systems demonstrated a link between carbon fixation pathways (with different potential fractionation factors) present and biomass $\delta^{13}C$ values, suggesting signals in the rock record are likely influenced by the predominant autotrophic community members present (Havig et al., 2011). Fractionation values (biomass $\delta^{13}C$ values found in **Table 2** minus DIC $\delta^{13}C$ values found in **Table 1**) for the microbial morphologies studied ranged from −13.0‰ for Site 1A green filaments to −25.9‰ for Site

1B green mat. Fractionation values differed slightly from their absolute values due to the DIC $\delta^{13}C$ values for the hot springs studied being close to zero (1.98 to −2.52‰, **Table 1**). These DIC values are similar to other analyses of DIC $\delta^{13}C$ values reported for silica-saturated hot springs located within or near the 640 Ka caldera boundary in Yellowstone National Park (Havig, 2009; Havig et al., 2011). We used these fractionation ranges to compare our results to those observed in the rock record. Assuming average ocean DIC $\delta^{13}C$ values through

time have remained nearly constant at ∼0‰ (Havig et al., 2017 and references therein), and that organic carbon in the rock record predominantly represents fractionation values by autotrophic microorganisms (Havig et al., 2011, 2017), we can plot known reported organic C $\delta^{13}C$ values of filaments, mats, and stromatolites from the rock record for comparison. Average values of rock units with stromatolites, mats, and filaments present reported in the literature overlap with fractionation values reported in this study (**Figure 4**), suggesting relationships

FIGURE 4 | Literature organic carbon $\delta^{13}C$ data from hydrothermal systems (left) and the rock record (right). **Left:** Comparison of results from this study (closed squares) to literature (closed circles) organic carbon $\delta^{13}C$ values for hydrothermal biomass, plotted against temperature. Phototrophic communities are in black, chemotrophic in gray. Literature values from Estep (1984), van der Meer et al. (2000), Havig et al. (2011), Jennings et al. (2017). **Right:** Average literature organic carbon $\delta^{13}C$ values for rock units with stromatolites (filled diamonds) or filaments and mats (open diamonds), with standard deviations for units with more than one analysis. The gray shaded area indicates the range of values of organic carbon $\delta^{13}C$ values from this study. Literature values are provided as part of the Supplementary Online Material and are from Eichmann and Schidlowski (1975); Schidlowski et al. (1975); Barghoorn et al. (1977); Hayes et al. (1983); Kaufman et al. (1991); Strauss and Beukes (1996); Melezhik et al. (1997); Watanabe et al. (1997); House et al. (2000); Sreenivas et al. (2001); Ueno et al. (2001); Westall et al. (2001, 2006a,b); Noffke et al. (2003, 2006); Ono et al. (2006); Thomazo et al. (2009); Yoshiya et al. (2012); Williford et al. (2016).

FIGURE 5 | Cartoon illustrating the relationship between productivity and preservation potential for microbial community morphologies sampled in this study.

observed in modern sites may provide insight into processes recorded in the rock record. In our study of modern structures, mats, filaments and stromatolites were indistinguishable based on $\delta^{13}C$ values yet we observed significant differences in primary productivity.

Microbial Assemblages in Filaments, Mats, and Stromatolites

The phototrophic filaments, mats and stromatolites are comprised largely of sequences affiliated with Cyanobacteria including OTUs most closely related to filamentous species of *Fischerella, Leptolyngbya, Arthronema,* and *Thermosynechococcus* spp. which are found in hot springs with temperatures similar to those reported in this study. Bacterial 16S rRNA OTUs affiliated with FAPs of the phylum *Chloroflexi* were also recovered from mat and stromatolite samples. These data suggest multiple filament-forming species comprise these structures. Sequences affiliated with the mat forming cyanobacteria *Chlorogloeopsis* were also recovered from the stromatolite samples as well as diatoms. In addition to these structure-forming species, we also recovered abundant OTUs affiliated with unicellular cyanobacteria and photoautotrophic *Chlorobi*. The recovery of diverse photoautotrophs from the stromatolite is consistent with studies of Sharkbay stromatolites and modern freshwater stromatolites from the Ruidera Pools Natural Park, Spain and YNP where sequences of both Cyanobacteria and Chloroflexi were recovered (Papineau et al., 2005; Santos et al., 2010; Berelson et al., 2011; Pepe-Ranney et al., 2012). These results indicate cyanobacterial-dominated mats, filaments, and stromatolites can be comprised of functionally similar assemblages (abundant oxygenic photoautotrophs), that vary in community composition at the OTU level as well as primary productivity potential and overall morphology. In contrast, the purple filaments from Site 3 were largely eukaryotic, with the majority of sequences related to the green alga *Zygogonium*. In this acidic system where no light-independent carbon fixation was observed, the photoautotrophic *Zygogonium* appear to be the major structure-forming species. This is consistent with the predominance of eukaryotic algae (rather than cyanobacteria) in low pH environments which support photosynthesis (Brock, 1973). In Site 4, the majority of sequences recovered were affiliated with the filamentous autotrophic Aquificae *Sulfurihydrogenibium* suggesting this bacterium is responsible for filament formation in this environment. Aquificae are common in YNP environments, particularly those above 73°C, the upper temperature limit of phototrophs. Our data do not reveal clear trends in diversity with morphology, geochemistry, or productivity—bacterial diversity was highest in samples from Site 1, Site 2, and Site 3 whereas archaeal diversity was highest in the green mats from Site 2 and lowest in filaments from Site 3 and 4. Eukaryotic diversity was lower in general but this may be due to geochemical conditions that generally preclude eukaryotes in our sample sites (particularly Site 4). Our results suggest mat, filament, and stromatolite structures throughout Earth's history have been comprised of varying degrees of microbial diversity and function, dictated largely by environmental conditions (particularly for

mats and filaments), underscoring the need for studies of extant structures. Collectively, our isotopic data and community composition data are consistent with previous ambiguities (i.e., similar morphologies exist in different environments; carbon fixation pathways can produce biomass that is indistinguishable; e.g., Havig, 2009; Havig et al., 2011, 2017) and also highlights differences in potential primary productivity that should be considered when interpreting the rock record.

Microbial Community Productivity and Conceptual Model

Stromatolites have been readily preserved in the rock record since the Archean (e.g., van Kranendonk et al., 2008; Wacey, 2010; Nutman et al., 2016; Djokic et al., 2017), but filaments and mats have not been as well preserved, potentially obfuscating their role in carbon uptake and oxygen production in the past. Through studying multiple microbial community macrostructures within a single hot spring, we relate morphology to carbon uptake, and estimate oxygenic photosynthetic production of. For filaments, mats, and stromatolites found at Site 1, the stromatolites (Site 1D) had the lowest carbon uptake rates and the lowest inferred O_2 production. The two photosynthetic mats present (Sites 1B and 1C) exhibited higher rates of carbon uptake (2.0–3.4 times greater) and associated oxygenic photosynthesis O_2 production that were greater than the stromatolite sample. We measured the highest rate of carbon uptake (nearly an order of magnitude greater than the stromatolite sample) and oxygenic photosynthesis O_2 production in the photosynthetic filaments at Site 1A. We illustrate these results with a conceptual model of the observed relationship between productivity and preservation potential (**Figure 5**). Our results suggest a negative correlation between preservation potential and productivity: phototrophic filaments are more productive but have the lowest preservation potential whereas low productivity stromatolites have the highest preservation potential.

CONCLUSIONS

Here we present primary productivity and community composition data for filaments, mats, and stromatolites which are observed in the rock record and attributed to life. We demonstrate significant differences in primary productivity between structures from the same hot spring despite similarities in microbial community structure (at the Phylum level) and geochemistry. Our data highlight important differences in primary productivity between structures with ambiguous biomass $\delta^{13}C$ values and suggest stromatolites may represent low productivity end members of phototrophic microbial community compositions. Collectively, these data underscore the need to consider a larger role for microbial mats and filaments in carbon fixation and O_2 generation during the Archean and Proterozoic.

AUTHOR CONTRIBUTIONS

TH and JH designed the study, collected samples, and performed the field work. CS completed the laboratory analyses. CS, JH, and

TH analyzed and interpreted the data. All authors contributed to writing and editing the manuscript.

ACKNOWLEDGMENTS

SUPPLEMENTARY MATERIAL

The Supplementary Material for this article can be found online at: https://www.frontiersin.org/articles/10.3389/feart.2017.00097/full#supplementary-material

REFERENCES

Albertsen, M., Karst, S. M., Ziegler, A. S., Kirkegaard, R. H., and Nielsen, P. H. (2015). Back to basics – the influence of DNA extraction and primer choice on phylogenetic analysis of activatedsludge communities. *PLoS ONE* 10:e0132783. doi: 10.1371/journal.pone.0132783

Allwood, A. C., Walter, M. R., Kamber, B. S., Marshall, C. P., and Burch, I. W. (2006). Stromatolite reef from the Early Archaean era of Australia. *Nature* 441, 714–718. doi: 10.1038/nature04764

Apprill, A., McNally, S., Parsons, R., and Weber, L. (2015). Minor revision to V4 region SSU rRNA 806R gene primer greatly increases detection of SAR11 bacterioplankton. *Aquat. Microb. Ecol.* 75, 129–137. doi: 10.3354/ame01753

Barghoorn, E. S., Knoll, A. H., Dembicki, H., and Meinschein, W. G. (1977). Variation in stable carbon isotopes in organic matter from the gunflint iron formation. *Geochim. Cosmochim. Acta* 41, 425–430. doi: 10.1016/0016-7037(77)90271-X

Barns, S. M., Delwiche, C. F., Palmer, J. D., and Pace, N. R. (1996). Perspectives on Archaeal diversity, thermophily and monophyly from environmental rRNA sequences. *Proc. Natl. Acad. Sci. U.S.A.* 93, 9188–9193. doi: 10.1073/pnas.93.17.9188

Barns, S. M., Fundyga, R. E., Jeffries, M. W., and Pace, N. R. (1994). Remarkable archaeal diversity detected in a Yellowstone National Park hot spring environment. *Proc. Natl. Acad. Sci. U.S.A.* 91, 1609–1613. doi: 10.1073/pnas.91.5.1609

Bauld, J., Chambers, L. A., and Skyring, G. W. (1979). Primary productivity, sulfate reduction and sulfur isotope fractionation in algal mats and sediments of Hamelin pool, Shark Bay, W.A. *Aust. J. Mar. Freshwater Res.* 30, 753–764. doi: 10.1071/MF9790753

Benzerara, K., Skouri-Panet, F., Li, J., Férard, C., Gugger, M., Laurent, T., et al. (2014). Intracellular Ca-carbonate biomineralization is widespread in cyanobacteria. *Proc. Natl. Acad. Sci. U.S.A.* 111, 10933–10938. doi: 10.1073/pnas.1403510111

Berelson, W. M., Corsetti, F. A., Pepe-Ranney, C., Hammond, D. E., Beaumont, W., and Spear, J. R. (2011). Hot spring siliceous stromatolites from Yellowstone National Park: assessing growth rate and laminae formation. *Geobiology* 9, 411–424. doi: 10.1111/j.1472-4669.2011.00288.x

Bosak, T., Liang, B., Wu. T. D., Templer, S. P., Evans, A., Vali, H. (2012). Cyanobacterial diversity and activity in modern conical microbialites. *Geobiology* 10, 384–401. doi: 10.1111/j.1472-4669.2012.00334.x

Boyd, E. S., Fecteau, K. M., Havig, J. R., Shock, E. L., and Peters, J. W. (2012). Modeling the habitat range of phototrophs in Yellowstone National Park: toward the development of a comprehensive fitness landscape. *Front. Microbiol.* 3:221. doi: 10.3389/fmicb.2012.00221

Brock, T. D. (1973). Lower pH limit for the existence of blue-green algae: evolutionary and ecological implications. *Science* 179, 480–483. doi: 10.1126/science.179.4072.480

Brock, T. D., Brock, K. M., Belly, R. T., and Weiss, R. L. (1972). *Sulfolobus*: a new genus of sulfur-oxidizing bacteria living at low pH and high temperature. *Archiv. Mikrobiol.* 84, 54–68. doi: 10.1007/BF00408082

Buick, R. (1990). Microfossil Recognition in Archean Rocks: an appraisal of spheroids and filaments from a 3500 M.Y. old chert-barite unit at North Pole, western Australia. *Palaios* 5, 441–459. doi: 10.2307/3514837

Caporaso, J. G., Lauber, C. L., Walters, W. A., Berg-Lyons, D., Huntley, J., Fierer, N., et al. (2012). Ultra-high-throughput microbial community analysis on the Illumina HiSeq and MiSeq platforms. *ISME J.* 6, 1621–1624. doi: 10.1038/ismej.2012.8

Castelle, C. J., Wrighton, K. C., Thomas, B. C., Hug, L. A., Brown, C. T., Wilkins, M. J., et al. (2015). Genomic expansion of domain Archaea highlights roles for organisms from new phyla in anaerobic carbon cycling. *Curr. Biol.* 25, 690–701. doi: 10.1016/j.cub.2015.01.014

Castenholz, R. W. (1977). The effect of sulfide on the blue-green algae of hot springs II. Yellowstone National Park. *Microb. Ecol.* 3, 79–105. doi: 10.1007/BF02010399

Castenholz, R. W. (1978). "The biogeography of hot springs algae through enrichment cultures," in *Symposium: Experimental Use of Algal Culture in Limnology 26-28 October 1976,* (Sandefjord: Internationale Vereinigung fur Theoretische und Angewandte Limnologie, Mittelungen, no. 21).

Coman, C., Drugǎ, B., Hegedus, A., Sicora, C., and Dragoş, N. (2013). Archaeal and Bacterial diversity in two hot spring microbial mats from a geothermal region in Romania. *Extremophiles* 17, 523–534. doi: 10.1007/s00792-013-0537-5

Comeau, A. M., Li, W. K., Tremblay, J. É., Carmack, E. C., and Lovejoy, C. (2011). Arctic ocean microbial community structure before and after the 2007 record sea ice minimum. *PLoS ONE* 6:e27492. doi: 10.1371/journal.pone.0027492

Djokic, T., Van Kranendonk, M. J., Campbell, K. A., Walter, M. R., and Ward, C. R. (2017). Earliest signs of life on land preserved in Ca. 3.5 ga hot spring deposits. *Nat. Commun.* 8:15263. doi: 10.1038/ncomms15263

Dodd, M. S., Papineau, D., Grenne, T., Slack, J. F., Rittner, M., Pirajno, F., et al. (2017). Evidence for early life in Earth's oldest hydrothermal vent precipitates. *Nature* 543, 60–64. doi: 10.1038/nature21377

Edgar, R. C., Haas, B. J., Clemente, J. C., Quince, C., and Knight, R. (2011). UCHIME improves sensitivity and speed of chimera detection. *Bioinformatics* 27, 2194–2200. doi: 10.1093/bioinformatics/btr381

Eichmann, R., and Schidlowski, M. (1975). Isotopic fractionation between coexisting organic carbon—carbonate pairs in Precambrian sediments. *Geochim. Cosmochim. Acta* 39, 585–595. doi: 10.1016/0016-7037(75)90004-6

Engel, A. S., Lee, N., Porter, M. L., Stern, L. A., Bennett, P. C., and Wagner, M. (2003). Filamentous 'epsilonproteobacteria' dominate microbial mats from sulfidic cave springs. *Appl. Environ. Microbiol.* 69, 5503–5511. doi: 10.1128/AEM.69.9.5503-5511.2003

Engel, A. S., Porter, M. L., Stern, L. A., Quinlan, S., and Bennett, P. C. (2004). Bacterial diversity and ecosystem function of filamentous microbial mats from aphotic (cave) sulfidic springs dominated by chemolithoautotrophic "Epsilonproteobacteria". *FEMS Microbiol. Ecol.* 51, 31–53. doi: 10.1016/j.femsec.2004.07.004

Estep, M. L. F. (1984). carbon and hydrogen isotopic compositions of algae and bacteria from hydrothermal environments, Yellowstone National Park. *Geochim. Cosmochim. Acta.* 48, 591–599. doi: 10.1016/0016-7037(84)90287-4

Everroad, R. C., Otaki, H., Matsuura, K., and Haruta, S. (2012). Diversification of bacterial community composition along a temperature gradient at a thermal spring. *Microbes Environ.* 27, 374–381. doi: 10.1264/jsme2.ME11350

Fecteau, K. M. (2016). *Organic Carbon in Hydrothermal Systems: From Phototrophy to Aldehyde Transformations.* Ph.D. dissertation, Arizona State University, Tempe, Arizona.

Ferreira, A. C., Nobre, M. F., Rainey, F. A., Silva, M. T., Wait, R., Burghardt, J., et al. (1997). Deinococcus *Geothermalis* sp. nov. and Deinococcus *Murrayi* sp. nov., two extremely radiation-resistant and slightly thermophilic species from hot springs. *Int. J. Syst. Evol. Microbiol.* 47, 939–947. doi: 10.1099/00207713-47-4-939

Fournier, R. O. (1989). Geochemistry and dynamics of the Yellowstone National Park hydrothermal system. *Ann. Rev. Earth Planet. Sci.* 17, 13–53 doi: 10.1146/annurev.ea.17.050189.000305

French, K. L., Hallmann, C., Hope, J. M., Schoon, P. L., Zumberge, J. A., Hoshino, Y., et al. (2015). Reappraisal of hydrocarbon biomarkers in archean rocks. *Proc. Natl. Acad. Sci. U.S.A.* 112, 5915–5920. doi: 10.1073/pnas.1419563112

Garrity, G. M., Holt, J. G., Reysenbach, A.-L., Huber, H., Stetter, K. O., Zillig, W., et al. (2001). "Phylum Al. *Crenarchaeota* phy. nov.," in *Bergey's Manual*® *of Systematic Bacteriology*, eds D. R. Boone, R. W. Castenholz, and G. M. Garrity (New York, NY: Springer), 169–210.

Gomez-Saez, G. V., Pop Ristovam, P., Sievert, S. M., Elvert, M., Hinrichs, K.-U., and Bühring, S. I. (2017). Relative importance of chemoautotrophy for primary production in a light exposed marine shallow hydrothermal system. *Front. Microbiol.* 8:702. doi: 10.3389/fmicb.2017.00702

Havig, J. R. (2009). *Geochemistry of Hydrothermal Biofilms: Compositions of Biofilms in a Siliceous Sinter-Depositing Hot Spring.* Ph.D. dissertation, Arizona State University, Tempe, Arizona.

Havig, J. R., McCormick, M. L., Hamilton, T. L., and Kump, L. R. (2015). The behavior of biologically important trace elements across the oxic/euxinic transition of meromictic Fayetteville Green Lake, New York, USA. *Geochim. Cosmochim. Acta* 165, 389–406. doi: 10.1016/j.gca.2015.06.024

Havig, J. R., Hamilton, T. L., Bachan, A., and Kump, L. R. (2017). Sulfur and carbon isotopic evidence for metabolic pathway evolution and a four-stepped earth system progression across the archean and paleoproterozoic. *Earth Sci. Rev.* 174, 1–21. doi: 10.1016/j.earscirev.2017.06.014

Havig, J. R., Raymond, J., Meyer-Dombard, D. A., Zolotova, N., and Shock, E. L. (2011). Merging isotopes and community genomics in a siliceous sinter-depositing hot spring. *J. Geophys. Res. Biogeosci.* 116:G01005. doi: 10.1029/2010JG001415

Hayes, J. M., Wedeking, K. W., and Kaplan, I. R. (1983). "Precambrian organic geochemistry, preservation of the record," in *Earth's Earliest Biosphere: Its Origin and Evolution*, ed J. W. Schopf (Princeton, NJ: Princeton University Press), 93–133.

Hofmann, H. J. (1975). Stratiform precambrian stromatolites, Belcher Islands, Canada; relations between silicified microfossils and microstructure. *Am. J. Sci.* 275, 1121–1132. doi: 10.2475/ajs.275.10.1121

House, C. H., Schopf, J. H., McKeegan, K. D., Coath, C. D., Harrison, T. M., and Stetter, K. O. (2000). Carbon isotopic composition of individual precambrian microfossils. *Geology* 28, 707–710. doi: 10.1130/0091-7613(2000)28<707:CICOIP>2.0.CO;2

Hugenholtz, P., Pitulle, C., Hershberger, K. L., and Pace, N. R. (1998). novel division level bacterial diversity in a Yellowstone hot spring. *J. Bacteriol.* 180, 366–376.

Hügler, M., Huber, H., Molyneaux, S. J., Vetriani, C., and Sievert, S. M. (2007). Autotrophic CO_2 fixation via the reductive tricarboxylic acid cycle in different lineages within the phylum Aquificae: evidence for two ways of citrate cleavage. *Environ. Microbiol.* 9, 81–92. doi: 10.1111/j.1462-2920.2006.01118.x

Jannasch, H. W., and Wirsen, C. O. (1981). Morphological survey of microbial mats near deep-sea thermal vents. *Appl. Environ. Microbiol.* 41, 528–538.

Jennings, R. M., Moran, J. J., Jay, Z. J., Beam, J. P., Whitmore, L. M., Kozubal, M. A., et al. (2017). Integration of metagenomic and stable carbon isotope evidence reveals the extent and mechanisms of carbon dioxide fixation in high-temperature microbial communities. *Front. Microbiol.* 8:88. doi: 10.3389/fmicb.2017.00088

Jiménez, D. J., Andreote, F. D., Chaves, D., Montaña, J. S., Osorio-Forero, C., Junca, H., et al. (2012). Structural and functional insights from the metagenome of an acidic hot spring microbial planktonic community in the Colombian Andes. *PLoS ONE* 7:e52069. doi: 10.1371/journal.pone.0052069

Kan, J., Clingenpeel, S., Macur, R. E., Inskeep, W. P., Lovalvo, D., Varley, J., et al. (2011). Archaea in Yellowstonel lake. *ISME J.* 5, 1784–1195. doi: 10.1038/ismej.2011.56

Kanokratana, P., Chanapan, S., Pootanakit, K., and Eurwilaichitr, L. (2004). Diversity and abundance of bacteria and archaea in the bor khlueng hot spring in Thailand. *J. Basic Microbiol.* 44, 430–444. doi: 10.1002/jobm.2004 10388

Kato, S., Kobayashi, C., Kakegawa, T., and Yamagishi, A. (2009). Microbial communities in iron-silica-rich microbial mats at deep-sea hydrothermal fields of the southern Mariana trough. *Environ. Microbiol.* 11, 2094–2111. doi: 10.1111/j.1462-2920.2009.01930.x

Kaufman, A. J., Hayes, J. M., Knoll, A. H., and Germs, G. J. B. (1991). Isotopic compositions of carbonates and organic carbon from upper proterozoic successions in Namibia: stratigraphic variation and the effects of diagenesis and metamorphism. *Precambrian Res.* 49, 301–327. doi: 10.1016/0301-9268(91)90039-D

Klatt, C. G., Wood, J. M., Rusch, D. B., Bateson, M. M., Hamamura, N., Heidelburg, J. F., et al. (2011). Community ecology of hot spring cyanobacterial mats: predominant populations and their functional potential. *ISME J.* 5, 1262–1278. doi: 10.1038/ismej.2011.73

Knoll, A. H. (1985). Extraordinary fossil biotas: their ecological and evolutionary significance - exceptional preservation of photosynthetic organisms in silicified carbonates and silicified peats. *Phil. Trans. R. Soc. Lond. B* 311, 111–122. doi: 10.1098/rstb.1985.0143

Konhauser, K. O., Jones, B., Reysenbach, A.-L., and Renaut, R. W. (2003). Hot spring sinters: keys to understanding earth's earliest life forms. *Can. J. Earth Sci.* 40, 1713–1724. doi: 10.1139/e03-059

Kozich, J. J., Westcott, S. L., Baxter, N. T., Highlander, S. K., and Schloss, P. D. (2013). Development of a dual-index sequencing strategy and curation pipeline for analyzing amplicon sequence data on the miseq illumina sequencing platform. *Appl. Environ. Microbiol.* 79, 5112–5120. doi: 10.1128/AEM.01043-13

Logan, B. W., Rezak, R., and Ginsburg, R. N. (1964). Classification and environmental significance of algal stromatolites. *J. Geol.* 72, 68–83. doi: 10.1086/626965

Lynn, R., and Brock, T. D. (1969). Notes on the ecology of a species of *zygogonium* (kütz.) In Yellowstone National Park. *J. Phycol.* 5, 181–185. doi: 10.1111/j.1529-8817.1969.tb02600.x

Macalady, J. L., Lyon, E. H., Koffman, B., Albertson, L. K., Meyer, K., Galdenzi, S., et al. (2006). Dominant microbial populations in limestone-corroding stream biofilms, frasassi cave system, Italy. *Appl. Environ. Microbiol.* 72, 5596–5609. doi: 10.1128/AEM.00715-06

Maliva, R. G., Knoll, A. H., and Simonson, B. M. (2005). Secular change in the precambrian silica cycle: insights from chert petrology. *GSA Bull.* 117, 835–845. doi: 10.1130/B25555.1

Mata, S. A., Harwood, C. L., Corsetti, F. A., Stork, N. J., Eilers, K., Berelson, W. M., et al. (2012). Influence of gas production and filament orientation on stromatolite microfabric. *Palaios* 27, 206–219. doi: 10.2110/palo.2011.p11-088r

McDermott, T., and Skorupa, D. (2011). *Microbiology of Serpentine Hot Springs, Alaska.* MSU-233 J979111KJ9013. Bozeman, MT: Montana State University.

McMurdie, P. J., and Holmes, S. (2013). Phyloseq: an R package for reproducible interactive analysis and graphics of microbiome census data. *PLoS ONE* 8:e61217. doi: 10.1371/journal.pone.0061217

Melezhik, V. A., Fallick, A. E., Makarikhin, V. V., and Lyubtsov, V. V. (1997). Links between palaeoproterozoic palaeogeography and rise and decline of stromatolites: fennoscandian shield. *Precambrian Res.* 82, 311–348. doi: 10.1016/S0301-9268(96)00061-7

Meyer-Dombard, D. R., Shock, E. L., and Amend, J. P. (2005). Archaeal and bacterial communities in geochemically diverse hot springs of Yellowstone National Park, USA. *Geobiology* 3, 211–227. doi: 10.1111/j.1472-4669.2005.00052.x

Noffke, N., Eriksson, K. A., Hazen, R. M., and Simpson, E. L. (2006). A new window into early archean life: microbial mats in earth's oldest siliciclastic tidal deposits (3.2 Ga Moodies Group, South Africa). *Geology* 34, 253–256. doi: 10.1130/G22246.1

Noffke, N., Hazen, R., and Nhleko, N. (2003). Earth's earliest microbial mats in a siliciclastic marine environment (2.9 Ga Mozaan Group, South Africa). *Geology* 31, 673–676. doi: 10.1130/G19704.1

Northup, D. E., Melim, L. A., Spilde, M. N., Hathaway, J. J. M., Garcia, M. G., Moya, M., et al. (2011). lava cave microbial communities with mats and secondary mineral deposits: implications for life detection on other planets. *Astrobiology* 11, 601–618. doi: 10.1089/ast.2010.0562

Nutman, A. P., Bennett, V. C., Friend, C. R. L., Van Kranendonk, M. J., and Chivas, A. R. (2016). Rapid emergence of life shown by discovery

of 3,700-million-year-old microbial structures. *Nature* 537, 535–538. doi: 10.1038/nature19355

Oehler, J. H., and Schopf, J. W. (1971). Artificial microfossils: experimental studies of permineralization of blue-green algae in silica. *Science* 174, 1229–1231. doi: 10.1126/science.174.4015.1229

Ono, S., Beukes, N. J., Rumble, D., and Fogel, M. L. (2006). Early evolution of atmospheric oxygen from multiple-sulfur and carbon isotope records of the 2.9 Ga Mozaan group of the Pongola Supergroup, southern Africa. *SAJG* 109, 97–108. doi: 10.2113/gssajg.109.1-2.97

Ortiz-Alvarez, R., and Casamayor, E. O. (2016). High occurrence of Pacearchaeota and Woesearchaeota (Archaea superphylum DPANN) in the surface waters of oligotrophic high-altitude lakes. *Environ. Microbiol. Rep.* 8, 210–217. doi: 10.1111/1758-2229.12370

Pace, N. R. (1997). A molecular view of microbial diversity and the biosphere. *Science* 276, 734–740. doi: 10.1126/science.276.5313.734

Pachiadaki, M. G., Kallionaki, A., Dählmann, A., De Lange, G. J., and Kormas, K. A. (2011). diversity and spatial distribution of prokaryotic communities along a sediment vertical profile of a deep-sea mud volcano. *Microb. Ecol.* 62, 655–668. doi: 10.1007/s00248-011-9855-2

Papineau, D., Walker, J. J., Mojzsis, S., and Pace, N. R. (2005). Composition and structure of microbial communities from stromatolites of Hamelin Pool in Shark Bay, Western Australia. *Appl. Environ. Microbiol.* 71, 4822–4832. doi: 10.1128/AEM.71.8.4822-4832.2005

Pejler, B. (1995). "Relation to habitat in rotifers," in *Rotifera VII, Developments in Hydrobiology*, eds J. Ejsmont-Karabin and R. M. Pontin (Dordrecht: Springer), 267–278.

Pepe-Ranney, C., Berelson, W. M., Corsetti, F. A., Treants, M., and Spear, J. R. (2012). Cyanobacterial construction of hot spring siliceous stromatolites in Yellowstone National Park. *Environ. Microbiol.* 14, 1182–1197. doi: 10.1111/j.1462-2920.2012.02698.x

Podosokorskaya, O. A., Kadnikov, V. V., Gavrilov, S. N., Mardanov, A. V., Merkel, A. Y., Karnachuk, O. V., et al. (2013). Characterization of *Melioribacter Roseus* gen. nov., sp. nov., a novel facultatively anaerobic thermophilic cellulolytic bacterium from the class Ignavibacteria, and a proposal of a novel bacterial phylum Ignavibacteriae. *Environ. Microbiol.* 15, 1759–1771. doi: 10.1111/1462-2920.12067

Revsbach, N. P., and Ward, D. M. (1984). Microelectrode studies of interstitial water chemistry and photosynthetic activity in a hot spring microbial mat. *Appl. Environ. Microbiol.* 48, 270–275.

Reyes, K., Gonzalez, N. I. III., Stewart, J., Ospino, F., Nguyen, D., Cho, D. T., et al. (2013). Surface orientation affects the direction of cone growth by *Leptolyngbya* sp. Strain C1, a likely architect of coniform structures Octopus Spring (Yellowstone National Park). *Appl. Environ. Microbiol.* 79, 1302–1308. doi: 10.1128/AEM.03008-12

Reysenbach, A.-L., Banta, A., Civello, S., Daly, J., Mitchel, K., Lalonde, S., et al. (2005). "The *Aquificales* in yellowstone national park," in *Geothermal Biology and Geochemistry in Yellowstone National Park*, eds W. P. Inskeep, T. R. McDermott (Bozeman, MT: Thermal Biology Institute, Montana State University), 129–142.

Reysenbach, A.-L., and Shock, E. (2002). Merging genomes with geochemistry in hydrothermal ecosystems. *Science* 296, 1077–1082. doi: 10.1126/science.1072483

Riding, R. (2011). "Microbialites, stromatolites, and thrombolites," in *Encyclopedia of Geobiology, Encyclopedia of Earth Sciences Series*, eds J. Reitner and V. Thiel (Dordrecht: Springer), 635–654.

Robertson, C. E., Spear, J. R., Harris, J. K., and Pace, N. R. (2009). diversity and stratification of archaea in a hypersaline microbial mat. *Appl. Environ. Microbiol.* 75, 1801–1810. doi: 10.1128/AEM.01811-08

Saghaï, A., Gutiérrez-Preciado, A., Deschamps, P., Moreira, D., Bertolino, P., Ragon, M., et al. (2017). Unveiling microbial interactions in stratified mat communities from a warm saline shallow pond. *Environ. Microbiol.* 19, 2405–2421. doi: 10.1111/1462-2920.13754

Santos, F., Pena, A., Nogales, B., Soria-Soria, E., García del Cura, M. A., González-Martín, J. A., et al. (2010). Bacterial diversity in dry modern freshwater stromatolites from Ruidera Pools Natural Park, Spain*Syst. Appl. Microbiol.* 33, 209–221. doi: 10.1016/j.syapm.2010.02.006

Schidlowski, M., Eichmann, R., and Junge, C. E. (1975). Precambrian sedimentary carbonates: carbon and oxygen isotope geochemistry and

implications for the terrestrial oxygen budget. *Precambrian Res.* 2, 1–69. doi: 10.1016/0301-9268(75)90018-2

Schieber, J. (1998). Possible indicators of microbial mat deposits in shales and sandstones: examples from the mid-proterozoic belt supergroup, Montana, U.S.A. *Sediment. Geol.* 120, 105–124. doi: 10.1016/S0037-0738(98)00029-3

Schloss, P. D., Westcott, S. L., Ryabin, T., Hall, J. R., Hartmann, M., Hollister, E. B., et al. (2009). Introducing mothur: open-source, platform-independent, community-supported software for describing and comparing microbial communities. *Appl. Environ. Microbiol.* 75, 7537–7541. doi: 10.1128/AEM.01541-09

Schopf, J. W. (1993). Microfossils of the early archean apex chert: new evidence of the antiquity of life. *Science* 260, 640–646. doi: 10.1126/science.260.5108.640

Schopf, J. W., Kudryavtsev, A. B., Czaja, A. D., and Tripathi, A. B. (2007). Evidence of archean life: stromatolites and microfossils. *Precambrian Res.* 158, 141–155. doi: 10.1016/j.precamres.2007.04.009

Shock, E. L., Holland, M., Meyer-Dombard, D. R., and Amend, J. P. (2005). "Geochemical sources of energy for microbial metabolism in hydrothermal ecosystems: Obsidian Pool, Yellowstone National Park," in *Geothermal Biology and Geochemistry in Yellowstone National Park*, ed T. R. McDermott (Bozeman, MT: Montana State University), 95–112.

Song, Z.-Q., Wang, F.-P., Zhi, X.-Y., Chen, J.-Q., Zhou, E.-M., Liang, F., et al. (2013). Bacterial and archaeal diversities in Yunnan and Tibetan hot springs, China. *Environ. Microbiol.* 15, 1160–1175. doi: 10.1111/1462-2920.12025

Southgate, P. N. (1986). Depositional environment and mechanism of preservation of microfossils, upper proterozoic bitter springs formation, Australia. *Geology* 14, 683–686.

Spear, J. R., Walker, J. J., McCollom, T. M., and Pace, N. R. (2005). Hydrogen and bioenergetics in the Yellowstone geothermal ecosystem. *Proc. Natl. Acad. Sci. U.S.A.* 102, 2555–2560. doi: 10.1073/pnas.0409574102

Spear, R., and Corsetti, F. A. (2013). "The evolution of geobiology in the context of living stromatolites," in *Geological Society of America Special Papers*, Vol. 500 (McLean, VA: Geological Society of America), 549–565.

Sreenivas, B., Sharma, S. D., Kumar, B., Patil, D. J., Roy, A. B., and Srinivasan, R. (2001). Positive δ^{13}C excursion in carbonate and organic fractions from the Paleoproterozoic Aravalli Supergroup, Northwestern India. *Precambrian Res.* 106, 277–290. doi: 10.1016/S0301-9268(00)00131-5

Stal, L. J. (2012). "Cyanobacterial mats and stromatolites," in *Ecology of Cyanobacteria II*, ed B. Whitton (Dordrecht: Springer), 65–125.

Stockner, J. G. (1968). Algal growth and primary productivity in a thermal stream. *J. Fish. Res. Board Can.* 25, 2037–2058. doi: 10.1139/f68-181

Strauss, H., and Beukes, N. J. (1996). Carbon and Sulfur isotopic compositions of organic carbon and pyrite in sediments from the Transvaal supergroup, south Africa. *Precambrian Res.* 79, 57–71. doi: 10.1016/0301-9268(95)00088-7

Tank, M., Thiel, V., Ward, D. M., and Bryant, D. A. (2017). "A panoply of phototrophs: an overview of the thermophilic chlorophototrophs of the microbial mats of alkaline siliceous hot springs in Yellowstone National Park, WY, USA" in *Modern Topics in the Phototrophic Prokaryotes*, ed P. C. Hallenbeck (Cham: Springer International Publishing AG), 87–137.

Tekere, M., Lötter, A., Olivier, J., Jonker, N., and Venter, S. (2011). Metagenomic analysis of bacterial diversity of siloam hot water spring, Limpopo, south Africa. *Afr. J. Biotechnol.* 10, 18005–18012. doi: 10.5897/AJB11.899

Thomazo, C., Pinti, D. L., Busigny, V., Ader, M., Hashizume, K., and Philippot, P. (2009). Biological activity and the earth's surface evolution: insights from carbon, sulfur, nitrogen and iron stable isotopes in the rock record. *C. R. Palevol.* 8, 665–678. doi: 10.1016/j.crpv.2009.02.003

Tice, M. M., and Lowe, D. R. (2004). Photosynthetic microbial mats in the 3,416-myr-old ocean. *Nature* 431, 549–552. doi: 10.1038/nature02888

Tobler, D. J., and Benning, L. G. (2011). Bacterial diversity in five Icelandic geothermal waters: temperature and sinter growth rate effects. *Extremophiles* 15, 473. doi: 10.1007/s00792-011-0378-z

Ueno, Y., Isozaki, Y., Yurimoto, H., and Maruyama, S. (2001). carbon isotopic signatures of individual archean microfossils(?) from western Australia. *Int. Geol. Rev.* 43, 196–212. doi: 10.1080/00206810109465008

van der Meer, M. T. J., Schouten, S., de Leeuw, J. W., and Ward, D. M. (2000). Autotrophy of green non-sulphur bacteria in hot spring microbial mats:

biological explanations for isotopically heavy organic carbon in the geological record. *Environ. Microbiol.* 2, 428–435. doi: 10.1046/j.1462-2920.2000.00124.x

van Kranendonk, M. J., Philippot, P., Lepot, K., Bodorkos, S., and Pirajno, F. (2008). Geological setting of earth's oldest fossils in the ca. 3.5ga dresser formation, Pilbara Craton, western Australia. *Precambrian Res.* 167, 93–124. doi: 10.1016/j.precamres.2008.07.003

Wacey, D. (2010). Stromatolites in the ~3400 Ma strelley pool formation, western Australia: examining biogenicity from the macro-to the nano-scale. *Astrobiology* 10, 381–395. doi: 10.1089/ast.2009.0423

Watanabe, Y., Naraoka, H., Wronkiewicz, D. J., Condie, K. C., and Ohmoto, H. (1997). Carbon, nitrogen, and sulfur geochemistry of archean and proterozoic shales from the Kaapvaal Craton, south Africa. *Geochim. Cosmochim. Acta* 61, 3441–3459. doi: 10.1016/S0016-7037(97)00164-6

Westall, F., de Ronde, C. E. J., Southam, G., Grassineau, N., Colas, M., Cockell, C., et al. (2006a). implications of a 3.472–3.333 Gyr-old subaerial microbial mat from the barberton greenstone belt, south Africa for the UV environmental conditions on the early earth. *Philos. Trans. R. Soc. B* 361, 1857–1876. doi: 10.1098/rstb.2006.1896

Westall, F., de Vries, S. T., Nijman, W., Rouchon, V., Orberger, B., Pearson, V., et al. (2006b). "The 3.466 Ga "kitty's gap chert," an early archean microbial ecosystem," in *Special Paper 405: Processes on the Early Earth*, Vol. 405 (McLean, VA: Geological Society of America), 105–131.

Westall, F., de Wit, M. J., Dann, J., van der Gaast, S. J., de Ronde, C. E., and Gerneke, D. (2001). Early archean fossil bacteria and biofilms in hydrothermally-influenced sediments from the barberton greenstone belt, south Africa. *Precambrian Res.* 106, 93–116. doi: 10.1016/S0301-9268(00)00127-3

Williford, K. H., Ushikubo, T., Lepot, K., Kitajima, K., Hallmann, C., Spicuzza, M. J., et al. (2016). Carbon and sulfur isotopic signatures of ancient life and environment at the microbial scale: neoarchean shales and carbonates. *Geobiology* 14, 105–128. doi: 10.1111/gbi.12163

Yoshiya, K., Nishizawa, M., Sawaki, Y., Ueno, Y., Komiya, T., Yamada, K., et al. (2012). *In situ* iron isotope analyses of pyrite and organic carbon isotope ratios in the fortescue group: metabolic variations of a late archean ecosystem. *Precambrian Res.* 212, 169–193. doi: 10.1016/j.precamres.2012.05.003

Conflict of Interest Statement: The authors declare that the research was conducted in the absence of any commercial or financial relationships that could be construed as a potential conflict of interest.